SENSOR LAYOUT OPTIMIZATION USING GENETIC ALGORITHM FOR SNIPER LOCALIZATION SYSTEMS

A THESIS SUBMITTED TO
THE GRADUATE SCHOOL OF NATURAL AND APPLIED SCIENCES
OF
MIDDLE EAST TECHNICAL UNIVERSITY

BY

EMİR DOĞAN

IN PARTIAL FULFILLMENT OF THE REQUIREMENTS
FOR
THE DEGREE OF MASTER OF SCIENCE
IN
ELECTRICAL AND ELECTRONICS ENGINEERING

DECEMBER 2019

Approval of the thesis:

SENSOR LAYOUT OPTIMIZATION USING GENETIC ALGORITHM FOR SNIPER LOCALIZATION SYSTEMS

submitted by **EMİR DOĞAN** in partial fulfillment of the requirements for the degree of **Master of Science in Electrical and Electronics Engineering Department, Middle East Technical University** by,

Prof. Dr. Halil Kalıpçılar
Dean, Graduate School of **Natural and Applied Sciences** _____

Prof. Dr. İlkay Ulusoy
Head of Department, **Electrical and Electronics Eng.** _____

Prof. Dr. Tolga Çiloğlu
Supervisor, **Electrical and Electronics Eng., METU** _____

Examining Committee Members:

Prof. Dr. Umut Orguner
Electrical and Electronics Eng., METU _____

Prof. Dr. Tolga Çiloğlu
Electrical and Electronics Eng., METU _____

Prof. Dr. Kemal Leblebicioğlu
Electrical and Electronics Eng., METU _____

Assist. Prof. Dr. Sevinç Figen Öktem
Electrical and Electronics Eng., METU _____

Assist. Prof. Dr. Yakup Özkazanç
Electrical and Electronics Eng., Hacettepe Uni. _____

Date: 09.12.2019

I hereby declare that all information in this document has been obtained and presented in accordance with academic rules and ethical conduct. I also declare that, as required by these rules and conduct, I have fully cited and referenced all material and results that are not original to this work.

Name, Surname: Emir Doğan

Signature:

ABSTRACT

SENSOR LAYOUT OPTIMIZATION USING GENETIC ALGORITHM FOR SNIPER LOCALIZATION SYSTEMS

Doğan, Emir
Master of Science, Electrical and Electronics Engineering
Supervisor: Prof. Dr. Tolga Çiloğlu

December 2019, 93 pages

This thesis proposes sensor layout optimization for a sniper localization system based on acoustic signatures of firearms such as ballistic shockwave and muzzle blast. This thesis consists of three main parts as sniper localization system simulator, estimation framework, and sensor layout optimization. The simulator provides the sniper localization system outline, transmission model of acoustic signals, muzzle blast, and shockwave modeling. The estimation framework comprises of the direction of arrival estimation using time-domain delay and sum beamforming, the range and the location of the shooter. Sensor layout optimization which minimizes mean squared location error on a bounded region is performed using the genetic algorithm. Then, the performance of the optimized sensor layout and the uniform circular array is compared in terms of the shooter location error.

Keywords: Sniper Localization System, Sniper Localization System Simulator, Genetic Algorithm, Sensor Layout Optimization

ÖZ

ATIŞ YERİ TESPİT SİSTEMLERİ İÇİN GENETİK ALGORİTMA KULLANARAK SENSÖR YERLEŞİM OPTİMİZASYONU

Doğan, Emir
Yüksek Lisans, Elektrik ve Elektronik Mühendisliği
Tez Danışmanı: Prof. Dr. Tolga Çiloğlu

Aralık 2019, 93 sayfa

Bu tez, ateşli silahların ateşlenmesi sonucu ortaya çıkan balistik şok dalgası ve namlu patlaması akustik işaretlerini kullanarak atış yeri tespiti yapan sistemler için, sensor yerleşim optimizasyonu sunmaktadır. Atış yeri tespit sistemi simülasyonu, kestirim çerçevesi ve sensor yerleşim optimizasyonu tezin üç ana kısmını oluşturmaktadır. İlk olarak, atış yeri tespit sistemi taslağı, namlu patlaması ve şok dalgası modellemesi ve hava akustiği iletim modeli simulasyonu oluşturmaktadır. İkinci kısımda, zaman bölgesinde geciktir ve topla hüzme oluşturma yöntemine dayalı yön kestirimi ve atıcının menzil ve lokasyon kestirimi sağlanacaktır. Son olarak, ortalama karekök lokasyon hatasına dayalı sensor yerleşim optimizasyonu genetik algortima yöntemi kullanılarak uygulanmaktadır. Sonra, optimize edilmiş sensör yerleşimleri, düzgün dairesel sensor yerleşimleriyle lokasyon kestirimi performansı bakımından karşılaştırılmaktadır.

Anahtar Kelimeler: Atış Yeri Tespit Sistemi, Atış Yeri Tespit Sistemi Simülasyonu, Genetik Algoritma, Sensör Yerleşim Optimizasyonu

To my family,

ACKNOWLEDGEMENTS

Foremost, I would like to express my sincere and deepest gratitude to my supervisor Prof. Dr. Tolga Çiloğlu for his continued guidance, support, inspiring opinions and encouragement during my study. His advice and assistance enhance my studies, my personal development, and my experiences.

Also, I am deeply grateful to Dr. Alper Bereketli, Erdal Mehmetçik and my colleagues from ASELSAN A.Ş. for their contributions and motivations.

I am really grateful to TÜBİTAK for their financial support throughout my thesis study.

Furthermore, I am obliged to my parents Emel Doğan and Ahmet Bülent Doğan and my brother Mehmet Emre Doğan for their endless love, help, and belief throughout my thesis period and my entire life.

Most of all, I am deeply thankful to my dear lovely wife Zeynep Aybüke Doğan for her support, motivation and always being with me.

TABLE OF CONTENTS

LIST OF TABLES

TABLES

LIST OF FIGURES

FIGURES

LIST OF ABBREVIATIONS

ABBREVIATIONS

CRB	:	Cramer-Rao Bound
CRLB	:	Cramer-Rao Lower Bound
DAS	:	Delay and Sum
DOA	:	Direction of Arrival
dB	:	Decibel
GA	:	Genetic Algorithm
SNR	:	Signal to Noise Ratio
SPL	:	Sound Pressure Level
SLS	:	Side Lobe Suppression
SLSL	:	Side Lobe Suppression Level
HPB	:	Half-Power Beamwidth
TOA	:	Time of Arrival
UCA	:	Uniform Circular Array
MUSIC	:	Multiple Signal Classification
MC	:	Monte Carlo
ME	:	Mean Error
MSE	:	Mean Square Error

CHAPTER 1

INTRODUCTION

1.1. Sniper Localization Problem

Sniper localization is a crucial problem for both military defense and civilian security applications. When snipers present a severe threat to the military mission, estimating the location of the shooter relying on human senses without using any detection systems might be inadequate. In conventional battlefield situations, several days might be needed to eliminate the well-skilled shooters since they are capable of remaining invisible in the field. Therefore, such concerns in the battlefield and willingness to expand situational awareness enabled sniper localization systems to gain popularity, especially in recent years. This popularity directs researchers and companies to study on sniper localization problem to take precautions to the shooter with automatic sniper localization systems.

1.2. Variety of Sniper Localization Techniques

There are several types of sniper localization techniques which can detect signals such as sound, motion or light since gunfire is attributed with three main characteristics such as optical flash, muzzle blast and ballistic shock wave (Kastek et al., 2011). Firstly, optical flash, in other words, muzzle flash is the result of setting fire of explosive charge at the barrel of the gun and can be detected by optical sensors. However, optical flashes must be seen by the sensors, so they must be in the line of sight or else that limited line of sight because of insufficient natural light or obstacle between optical sensors and snipers such as rocks and trees prevent localization systems from the detection of the shooter. Also, such optical localization techniques have another drawback that using only optical flashes is not enough to localize the

shooter since these systems are just capable of estimating the bearing of the shooter. Therefore, the sensor network solution that enables the triangulation to estimate the location of the shooter is necessary. Secondly, muzzle blast and ballistic shockwave are the acoustic events of discharging of gunfire. Although muzzle blast is the result of explosive charge at the barrel, too and it generates an impulse acoustic sound wave, ballistic shockwave is the consequence of the projectile movement of the bullet through the air with supersonic speed. Furthermore, acoustic localization techniques are generally based on these acoustic signatures such as muzzle blast and shockwave signals to estimate the position of the shooter.

1.3. Concept of Acoustic Sniper Localization Systems

Although some acoustic sniper localization systems depend on only muzzle blast or only shockwave signal, most of the acoustic sniper localization systems are generally based on two consecutive acoustic signatures. The system based on only muzzle blast (Mäkinen et al., 2010) signal has some drawbacks as not being capable of distinguishing muzzle blast explosion from other explosion types and not being able to estimate the position of the shooter by itself and needing system network to localize the sniper. Also, the system based on only the shockwave signal (Danicki, 2006) cannot estimate the location of the shooter since it only detects the bearing of the shockwave that gives information about the bullet trajectory. By making a sensor network, this information might be useful to estimate the bearing and location of the shooter. As it is mentioned before, most common acoustic sniper localization systems are subject to both acoustic signatures such as muzzle blast and shockwave signals (Damarla et al., 2010). By using these two acoustic events, only one sniper localization system can estimate the position of the shooter without the necessity of the network system.

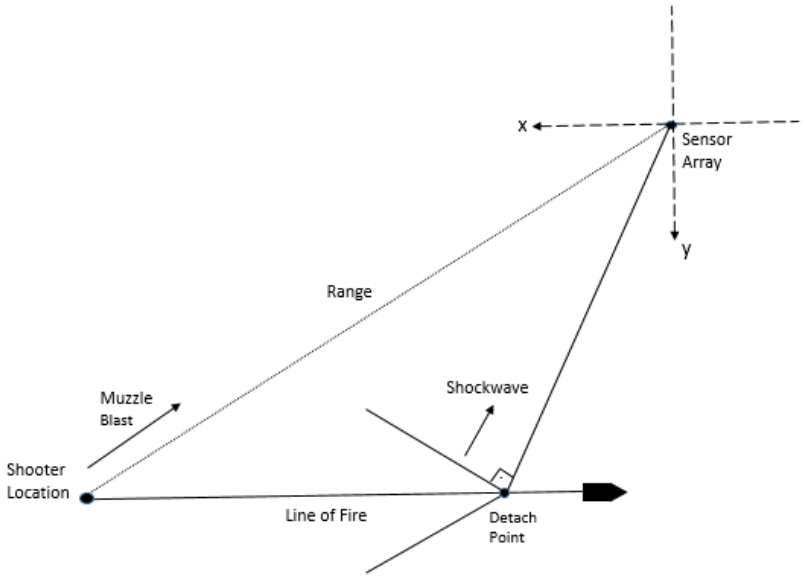

Figure 1.1: Concept of Acoustic Sniper Localization Systems

Figure 1.1 illustrates that the bearing of the muzzle blast signal gives the bearing of the shooter. However, the bearing of the ballistic shockwave signal gives information about the bearing of the detach point. Although it seems redundant information, direction and time of arrival difference between two acoustic signatures give a clue to find the range of the shooter. Then, using the bearing and range of the shooter, the acoustic sniper localization system figures out the location of the shooter.

1.4. Environmental Effects on Air Acoustics

In air acoustic fields, the speed of sound depends on the characteristics of the environment since air acoustic signals propagate through the air with the speed of sound. Also, the speed of sound can be regarded as a parameter of sniper localization systems since the propagation of sound depends on the features of the medium as humidity, temperature, pressure and air density. Changing the temperature affects air density. However, change in air density does not affect air pressure. When there is a

change in air pressure with constant temperature, the speed of the sound remains constant.

The speed of sound (c) in m/s is calculated using Equation 1.1 (Bohn, 1987).

$$c = \sqrt{\frac{1.4\ U\ C}{G}} \tag{1.1}$$

where U is the universal gas constant which is 8.314 J/(mol × K), G is the mean molecular weight of the gas which is 28.97 g/mol, and C is the air temperature of the medium in ºC.

Since U and G are constant, the speed of sound can be calculated with Equation 1.2 (Bohn, 1987).

$$c = c_0\sqrt{1 + C/273} \tag{1.2}$$

where c_0 is 331 m/s, and C is the air temperature of the medium in ºC.

1.5. Acoustic Sniper Localization Systems and Their Features

Although some mechanical sounds are associated with the hammer or the trigger, these sounds do not have any special interest in the system design. The sensor of the acoustic sniper localization systems are high sound pressure level (SPL) microphone since acoustic sniper localization systems are only subject to the detection and direction of muzzle blast and shockwave signals to estimate the location of the shooter and SPL of the shockwave signal might be very high that will be explained elaborately in Section 2.2. There are several types of acoustic sniper localization systems in terms of fields of use such as vehicle-mounted systems, fixed devices or wearable solutions. Vehicle-mounted and fixed sniper localization systems are similar to each other. The only difference between fixed solutions and vehicle-mounted devices is that vehicle-mounted systems must have a global positioning system (GPS) with two antennae to calculate the heading of the vehicle and consider the speed of the vehicle to estimate

shooter's location. Using the heading information, the system can estimate the location of the shooter, accurately.

There are internationally well known acoustic sniper localization systems such as BBN Boomerang (Boomerang III, 2019), Pilarw (Pilarw, 2019), Ferret (Bedard et al., 2003) and ASELSAN Spot (Aselsan, 2019) for fixed and vehicle-mounted solutions. The specification comparison of these systems is given in Table 1.1.

Table 1.1: Specification Comparison of Fixed Sniper Localization Systems

System Name	Dim.	Number of Sensors	Response Time	Azimuth Accuracy Error	Elevation Accuracy Error	Range Accuracy Error	Max. Range	Bullet Detection Range
ASELSAN Spot	25 x 25 cm	7	< 1.5 s	< 2.5°	< 2.5°	±10%	> 1200 m	100 m
BBN Boomerang	Dia: 56 cm	7	< 1.5 s	< 2.5°	< 2.5°	±10%	> 750 m	100 m
Pilarw	21 x 29 cm	4	3 s	± 2°	± 5°	±10% to ±20%	1500 m	Not given
Ferret	57 x 47 cm	4	< 1 s	2°	5°	±10% within 250m, ±30% greater than 250m	Up to an effective range of the weapon	200 m

There are internationally known wearable sniper localization systems such as BBN Boomerang Warrior (Boomerang Warrior-X, 2019), and QinetiQ Swats (Ears Swats, 2019). The performance comparison of wearable systems is given in Table 1.2.

Table 1.2: Specification Comparison of Wearable Sniper Localization Systems

System Name	Dimension	Number of Sensors	Response Time	Azimuth Accuracy Error	Range Accuracy Error	Maximum Range	Bullet Detection Range
BBN Boomerang Warrior	8 x 11 cm	4	< 1.5 s	< 7.5°	±20%	Not given	> 50 m
QinetiQ Swats	9 x 8 cm	4	< 0.5 s	± 7.5°	±10%	> 400 m	Not given

Tables 1.1 and 1.2 benchmark the comparisons of the main specifications of acoustic sniper localization systems for fixed and wearable solutions. The number of sensors (*M*) used in the given systems depends on the system configuration. Normally, $M > 1$ condition is enough to estimate the direction of the acoustic signals. However, to meet the system specifications, the number of sensors may change. The system performance given in the tables are very similar, but there is no specific information about the test conditions.

As it is seen in Table 1.1 and 1.2, the main difference between fixed solutions and wearable systems are about elevation specification since wearable solutions don't provide elevation information as distinct from fixed systems. Apart from elevation specifications, it can be stated that the performance criteria of wearable solutions are a little bit lower than the criteria of fixed solutions.

1.6. The Motivation of Study

The sniper localization system can be very useful in numerous fields such as civil defense, law enforcement, military convoy, unit protection, and protection of soldiers on the battlefield. They are generally based on acoustic signatures since the microphone sensor layout and network of sensor configuration are quite easier than optics or electromagnetic system setup as is mentioned in Section 1.2. Acoustic signatures of a sniper or any kind of weapons can be classified into two acoustic events. These acoustic events are muzzle blast that is the result of a sudden expansion of gas in the barrel of gun and shockwave that is a sudden rise in the air since the bullet moves at supersonic projectile towards the target. By detecting these acoustical signatures, the presence of the shooter that poses a serious threat in the war field can be detected even if the shooter fires only a single shot.

There are several different applications of the acoustic sniper localization systems. Although some of these systems are based on detecting only shockwave events and use sensor network to localize the shooter, a great majority of the systems utilizes both

muzzle blast and shockwave events as acoustic signatures of a gunshot. Furthermore, designing the sensor layout to improve the acquisition of acoustical data is important since shockwave and muzzle blast have distinctive acoustic signal types and differ from each other. It means that the success of the sniper localization systems also depends on the sensor layout configuration. Therefore, the motivation of study in this thesis is to find optimum sensor layout in terms of the final test result which is the shooter location estimation using the acoustic sniper localization system simulator.

1.7. Literature Review

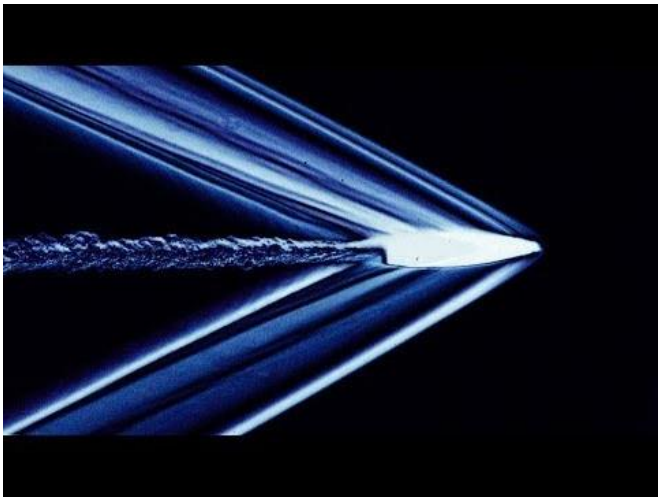

Figure 1.2: Travel of Bullet with Supersonic Projectile. The Ultra-slow Motion Photo Taken by Smarter Every Day (Audible, 2019)

Sniper localization system which estimates the shooter position based on the noisy environment is a research topic that has been conducted for many years. The main aim of the sniper localization system is to provide situational awareness for military defense and civilian security applications. The historical development of sniper localization systems has been reviewed in (Aguilar, 2013) in terms of technological development. There are several types of applications that can detect a wide spectrum of signal types such as sound, motion, and light (He et al., 2010). In air acoustics,

muzzle blast generated by the explosion of the gun and shockwave generated by the bullet moving at supersonic speed in the air are used as the acoustic signals to localize the shooter.

Fire detection and localization of small arms have been investigated widely and some of the researches are applied to the real gunshot localization systems. The Ferret system designed by Canadian forces utilizes the detection and estimation of the shockwave to determine if there is a shot (Bedard et al., 2003). After detecting the shockwave signal, the system waits for the muzzle blast to estimate the location of the shotgun. However, without any information about the muzzle blast, the system gives limited information and is not able to estimate the position of the shooter. The Ferret system can be regarded as an example of fixed or vehicle-mounted solutions. Also, wearable system solutions for the acoustic sniper localization systems are developed and they are commercially available for the defense industry applications (Raytheon, 2019). In some applications, shooter localization can be made using networked sensor arrays (Volygesi et al., 2007). In a system solution, a wireless sensor network based on the mobile counter-sniper system is established. The microphone array can be mounted on each helmet or shoulder of the soldier as a sensor node. Acoustic detection is achieved through a time of arrival data at nodes. In all applications, both shockwave and muzzle blast signals are used to estimate the position of the shooter. However, some of the sniper localization techniques are based solely on ballistic shockwaves to estimate the bearing of the shotgun (Sallai et al., 2013). In such a solution technique, since shockwave signal is not adequate to estimate the trajectory of the bullet and estimate the position of the shooter, a network between nearby smartphones is established to find the range and bearing of the shooter together.

To make localization of the shooter and show the location of the shooter to the allies, the global positioning system of smartphones can be utilized and wireless communication using an audio channel can be established. As a result, although there are fundamentally different applications in terms of whether using both or single acoustic signatures, many of the applications take both signatures into account to

estimate the position of the shooter by using direction of arrival (DOA) and time of arrival (TOA) estimation (Lédeczi et al., 2005; Lindgren et al., 2010).

Estimation of the shooter position fundamentally relies on the DOA and TOA of muzzle blast and shockwave signals. To estimate the location of the shooter, more accurately, direction estimation techniques for passive source signals that are received by spatially distributed microphones are provided. The most common direction arrival estimation techniques that are applied to acoustic sniper localization systems are a time difference of arrival (Khalid et al., 2013), multiple signal classification (MUSIC) (Zhang et al., 2014) and delay and sum (DAS) beamforming (Calderon et al., 2013).

Since the acoustic sniper detection system has two distinctive events namely the shockwave and muzzle blast, the relationship between these two signals reveals the position of the sniper. While the direction of the muzzle blast gives the direction of the shooter, the direction of the shockwave gives information about the trajectory of the bullet. The time difference of arrival and the bearing difference between these two signals is the result of the geometry of the shooting event. This geometry by considering the measured data as the arrival time of two signals and its propagation direction describes the acoustic sniper localization concept (Danicki et al., 2004).

Determination of the receiver sensor array layout for the most accurate position estimation is one of the basic problems of optimization. One of the ways to specify sensor locations is to use the geometric interpretation of the Cramer-Rao Bound (CRB) (Abel, 1990). The information inequality by using the Fisher Information matrix for bearing parameter is observed to find the bound for passive localization. For the passive localization problem, different sensor array arrangements are presented for the optimal bearing, range and position accuracy since all of these parameters are based on different types of inequality. For example, estimating the position for the passive source depends on bearing and range estimation. In such optimization cases, most commonly used antenna arrays to compare with the resulting

sensor layout after optimization are linear array (Carter, 1977; Carter, 1981) and uniform circular array (Kadan, 2018) with a fixed radius.

Even though most of the studies on finding optimal sensor placement are using the CRB inequality for some parameters, there are some different optimization criteria as low ambiguity of sensor arrangement (Sadler, 2009). In some cases, the array antenna is designed to make ambiguity of sensor array lower to avoid spurious responses in the spatial spectrum The main purpose of making ambiguity lower is to reduce the occurrence of false alarms. The cost function of this optimization method is concerning low ambiguity arrays for the direction-finding algorithm. When grating lobes, whose peak value is almost similar to the peak value of the main lobe that is the correct direction of the source signal, occur, virtually identical responses from several different directions are received. Therefore, spurious peaks occurred in the spatial spectrum and the peak of the true target is indistinctive in such a case. To prevent spurious peaks in the response of sensor array, the optimization based on low ambiguity is provided. Moreover, another application of optimization is to suppress side lobe levels to make directivity of array response even better (He et al., 2015). To suppress side lobes of the response of transducer array, the near field weight vector is optimized. Despite the difference between the center frequencies of air acoustic signals and ultrasound signals, the application, and purpose of side lobe suppression is the same as each other.

1.8. Main Contribution

Although the sniper localization system is recently a hot topic in the field of air acoustics, the amount of available information about sensor layout optimization for shockwave and muzzle blast signals and simulation of the sniper detection system is limited in the literature since these two acoustic signatures are specific to shooter localization systems. By taking the mentioned researches on acoustic sniper localization systems and optimization techniques into consideration and combining all

information, the main goal of this thesis is sensor layout optimization for the sniper localization systems using a genetic algorithm (GA). To improve the acquisition of acoustical data, and estimate the shooter location, more accurately, three priority contributions are discussed throughout the thesis: acoustic sniper localization system simulator, estimation frameworks that consist of DOA and TOA of acoustic events, range and location of the shooter, and sensor layout optimization for the acoustic shooter localization systems.

1.9. Thesis Organization

In light of the main contribution section, the layout of the thesis is organized as follows:

In Chapter 2, the implementation of the sniper localization system simulation is explained in detail. The parts of the simulation including the modeling of muzzle blast, and shockwave, channel model of air acoustic considering attenuation, and propagation of sound in the air are provided. Also, miss distance calculation, the concept of line of fire, and the detachment point of shockwave are discussed in this chapter. At the end of this chapter, inputs, and outputs of the sniper localization system simulation are given in detail.

In Chapter 3, estimation framework including DOA estimation and TOA estimation of muzzle blast and shockwave signals are provided. Also, the range estimation technique using DOA and TOA of acoustical signatures is discussed in this chapter.

Chapter 4 explains the optimization and genetic algorithm with the internal calculation behind the optimization techniques. The parameters of the optimization and its flow diagram are given at the end of the chapter.

In Chapter 5, the sensor layout optimization procedures such as side lobe suppression and location estimation using acoustic sniper localization system simulator described in Chapter 2, are provided. The performance comparison of the optimized sensor

layouts with the uniform circular array (UCA) is made in terms of shooter location estimation for a different number of sensors.

Finally, the conclusions of the study are discussed. Furthermore, some ideas and possible works that can be implemented in the future to advance the study are provided.

CHAPTER 2

SNIPER LOCALIZATION SYSTEM SIMULATOR

Sniper localization system simulator is generally based on the physics and measurements of muzzle blast and shockwave signals that are the consequence of gunfire. Sniper localization systems receive and process the acoustic signals using a sensor array to estimate DOA of muzzle blast and shockwave signals. The difference between times of shockwave and muzzle blast signals is required to estimate the range and the position of the shooter in addition to the DOA of acoustic events. An illustration of experimental data that is gathered on the field is given in Figure 2.1.

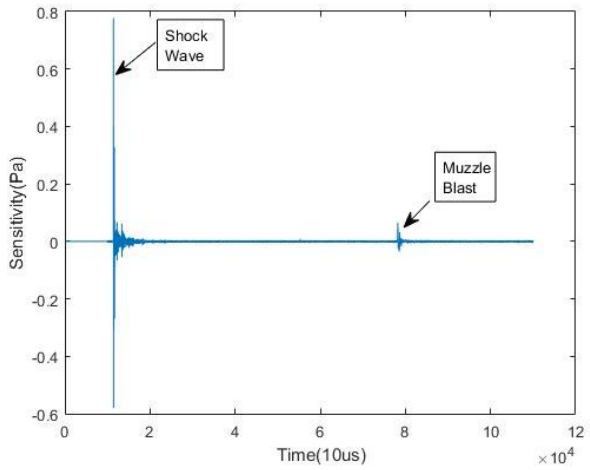

Figure 2.1: Experimental Data of Muzzle Blast and Shockwave

As shown in Figure 2.1, there are two distinctive acoustic measurements. First, the shockwave signal is received by the microphone array because the bullet moves towards the sensor at the supersonic speed which is almost twice the speed of the muzzle blast signal (Maher, 2007). However, the muzzle blast signal propagates at sound speed. Moreover, Figure 2.1 demonstrates the sound pressure level difference

between these two acoustic signals. Although the sound pressure level (SPL) of the supersonic bullet that passes one meter away from the microphones exceeds 140 dB (Snow, 1967), SPL of muzzle blast signal is 130 dB or even higher referenced by 1 meter in (Patterson et al., 1997). Another reason behind the SPL difference between two acoustic events is that the muzzle blast signal attenuates more through the air compared to the shockwave signals.

SPL in the air acoustics Equation can be described as the sound power that is transmitted from the sound source. The reference sound pressure level is 20μPa and reference distance to the sound source is 1 meter in Equation 2.1. SPL Equation is given below:

$$SPL\ in\ air = 20 \log\left(\frac{P}{20 \times 10^{-6} Pa}\right) dB \quad rel\ 20\ \mu\text{Pa}\ @1\text{m} \tag{2.1}$$

where P is the sound pressure of source signal in Pa. Figure 2.2 illustrates the TOA difference between two different microphones of a sensor array. By using the time difference between sensor nodes, the DOA of acoustic signals is estimated. Details of the DOA algorithm are elaborately explained in Chapter 3 which is the estimation framework.

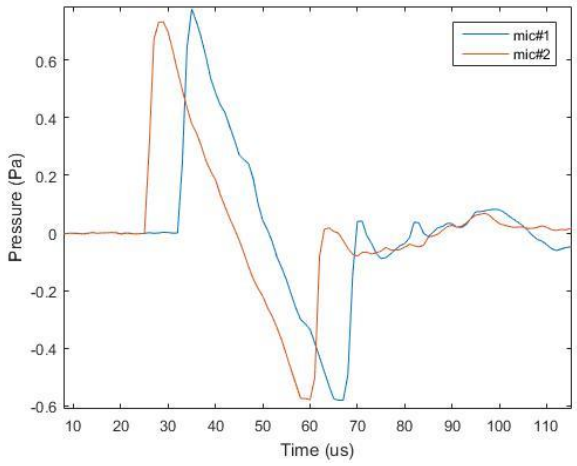

Figure 2.2: Shockwave Signal Example Received by Two Different Microphones

Figure 2.3 illustrates all information on the geometry of the sniper localization system outline. In Figure 2.3, the sensor array is located at the origin of the coordinate axis, b is the miss distance, R is the range of the shooter, β is the Mach angle which is the angle between the bullet trajectory and trajectory of the shockwave signal, the azimuth angle of muzzle blast is θ_{MB}, and the azimuth angle of shockwave signal is θ_{SW}.

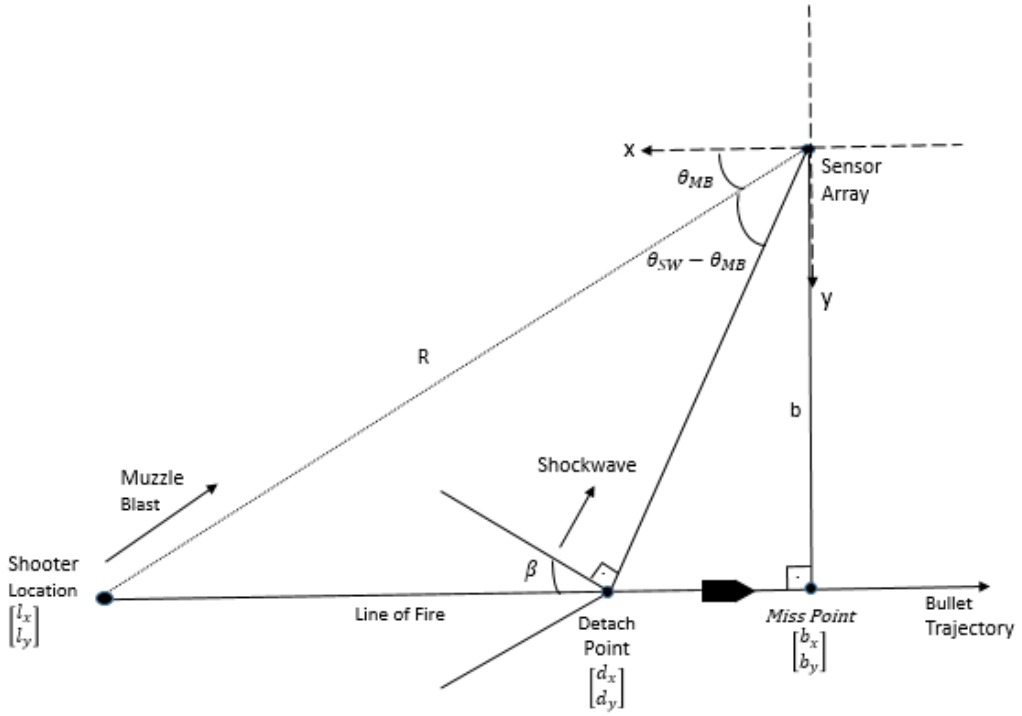

Figure 2.3: The Sniper Localization System Outline

The sniper localization system simulator consists of several parts as modeling of muzzle blast as described in Section 2.1, modeling of shockwave as described in Section 2.2, true range and azimuth of the shooter calculation, arranging the miss distance, drawing the line of fire, calculation of the detachment point of shockwave, calculation of true azimuth angle for muzzle blast and shockwave, the propagation of acoustic signals, absorption of acoustic signals, Signal-to-Noise Ratio (SNR) calculation and adding noise to the acoustic signals. Firstly, the sensor array is

centered at the origin and sensor location of an array is transformed from spherical coordinate to Cartesian coordinate. Let's assume that $\boldsymbol{B}$ is a *2* x *M* sensor position matrix.

$$\boldsymbol{B} = [\boldsymbol{p}_1 \quad \boldsymbol{p}_2 \quad \cdots \quad \boldsymbol{p}_M] = \begin{bmatrix} x_1 & x_2 & \cdots & x_M \\ y_1 & y_2 & \cdots & y_M \end{bmatrix} \tag{2.2}$$

where *M* is the number of sensors, $\boldsymbol{p}_k$ is the position vector of k^{th} sensor consisting of x_k, and y_k which are the Cartesian coordinates in meters.

The geometry of a sensor array in two dimensions is shown in Figure 2.4. In this figure, the locations of the sensor array element are given in the Cartesian coordinate.

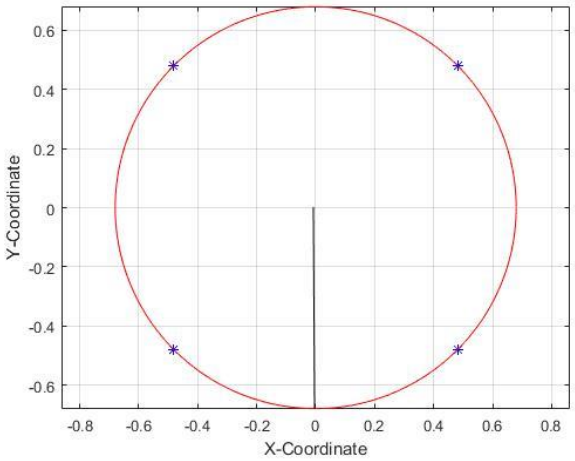

Figure 2.4: UCA with 4 Sensors when $r = \lambda$

2.1. Modeling of Muzzle Blast Signal

Muzzle blast is the result of the gas explosion at the barrel of the gun. In such an explosion at the barrel, even though acoustic energy spreads in all directions from the gunfire, SPL is at the highest rate in the direction of the gun barrel. At 1 meter, the approximate SPL is 130 dB or even higher as it is mentioned before and the SPL measured by the microphone is inversely proportional to the distance between the shooter and the microphone array for the muzzle blast signal (Maher, 2007).

Moreover, the criteria for discriminating between near-field and far-field assumptions are stated as $R > \pi a^2/\lambda$ where R is the distance between the source signal and sensor in meters, a is the radius of sensor layout in meters and λ is the acoustic wavelength (Foote, 2014) in meters. Since the distance between the source signal and sensor is quite larger than $\pi a^2/\lambda$ which is approximately 6 cm where a and λ are 11 cm and 68 cm, respectively described in Chapter 5, it is assumed that the muzzle blast is regarded as a planar wave.

The waveform features of muzzle blast are the positive phase duration, the negative phase duration which is the rise time and the peak amplitude since it is an explosion in the air (Beck et al., 2011). The positive phase duration is the time duration required for the muzzle blast signal pressure to go from peak pressure to the ambient noise level. The negative phase duration is the time duration when the muzzle blast signal pressure is below the ambient noise level. The rise time is the time duration for the muzzle blast signal pressure rise from the ambient noise level to the peak value of signal pressure. The model of the muzzle blast is given using Friedlander Equation (Beck et al., 2011) is as follows:

$$P_{\mathrm{m}}(t) = P_0 + P_{\mathrm{s}}\left(1 - \frac{t}{T_0}\right)e^{-\frac{gt}{T_0}} \tag{2.3}$$

where P_{m} is the measured pressure in Pa, P_0 is the ambient level of pressure in Pa, P_{s} is the peak overpressure in Pa, T_0 is the positive phase duration in s, and g is the exponential decay rate. The output of the function is pressure (Pa) depending on time (s). Since the ambient pressure is not measured by microphones, it is subtracted from the acoustic signal of each channel.

Sound pulses of small firearm muzzle blast last for 3-5 ms with a high SPL (Maher, 2007) and center frequency of muzzle blast is between 300 Hz and 1 kHz citing in Mays, 2001). Furthermore, detection of muzzle blast is not always easy. The shooter may utilize a silencer to suppress the high SPL at the gun barrel. Further, because of the propagation loss and ambient noise, the SNR of muzzle blast drops significantly

before it arrives at the sensor array. Therefore, these conditions are regarded as the challenges of muzzle blast detection. The muzzle blast model based on Friedlander (Beck et al., 2011) is illustrated in Figure 2.5.

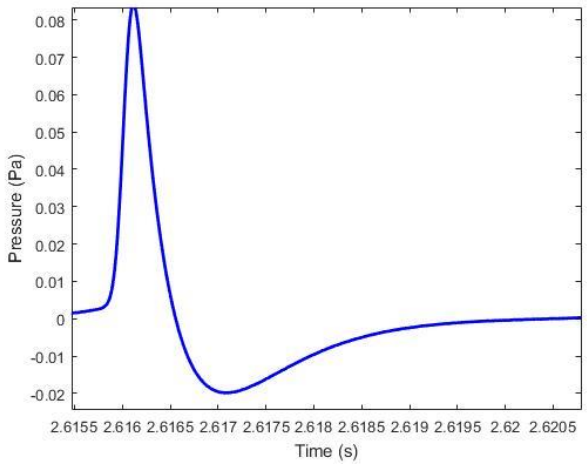

Figure 2.5: Friedlander Muzzle Blast Model

The values of the parameters presenting muzzle blast signal illustrated in Figure 2.5 are listed in Table 2.1.

Table 2.1. The Parameters of the Muzzle Blast Signal

Parameter	Value
Ambient Pressure (P_0)	101 Pa
Peak Overpressure (P_s)	343 m/s
Positive Phase Duration (T_0)	20%
Exponential Decay Rate (g)	1 atm
Center Frequency (f_c)	300 Hz – 1 kHz
Sampling Frequency (f_s)	50 kHz

2.2. Modeling of Shockwave Signal

When a bullet moves at supersonic speed, the sudden pressure change in the air occurs. This pressure change is caused by the ballistic shockwave. The shape of the ballistic shockwave resembles N-wave in the time domain representation as shown in Figure 2.6.

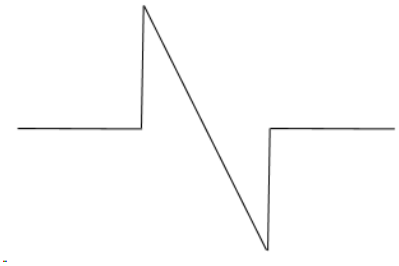

Figure 2.6: N-wave

The geometric representation of the ballistic shockwave movement is shown in Figure 2.7.

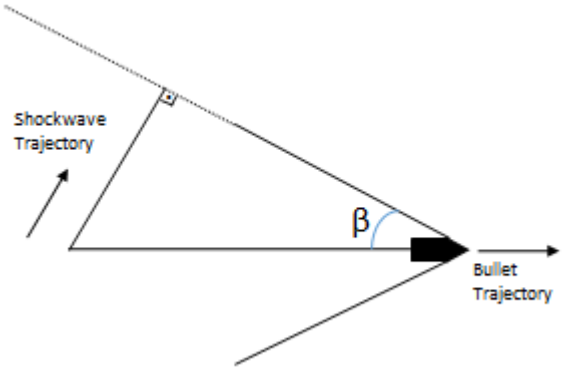

Figure 2.7: Bullet & Shockwave Trajectory

When there is a shot fired by a gun, the molecules in the air are disturbed and move around the bullet of the gun. When the bullet of the gun projectiles at very high speed as higher than sound speed, the energy of the bullet compresses the air and changes the density of the air locally. This compressibility effect of bullet changes the amount

of force. Therefore, the ratio of the speed of the bullet to the sound speed in the air determines the magnitude of the compressibility effect. This ratio is named Mach number (M_{mach}). The formula of the Mach number is given by Equation 2.4 (Maher, 2006):

$$M_{\text{mach}} = v/c \tag{2.4}$$

where v is the instantaneous bullet speed in m/s, and c is the sound speed in m/s. When Mach number is greater than 1 for the instantaneous bullet velocity, it means that the bullet moves at supersonic projectile.

In Figure 2.7, the shockwave signal spreads as a planar wave by forming a cone centered at the bullet as shown. The angle (β) between the bullet trajectory and vertex of the cone that is the direction of shockwave at sound speed is calculated with Equation 2.5 (Maher, 2006).

$$\beta = \arcsin\left(\frac{1}{M_{\text{mach}}}\right) \tag{2.5}$$

where M_{mach} is the Mach number, β is the Mach angle in radians.

When the bullet moves at its projector, the speed of the bullet that depends on the features of the gun decreases slowly. Moreover, according to the far-field and near-field assumption criteria that are mentioned before in the muzzle blast section, shockwave is taken into consideration as a planar wave, similar to muzzle blast since the distance between detachment point of shockwave and sensor array is quite larger than $\pi a^2/\lambda$ where R is the distance between source signal and sensor in meters, a is the radius of sensor layout in meters and λ is the acoustic wavelength in meters.

The shockwave signal depends on the miss distance to the sensor array, amplitude variations of ballistic shock, and novel measurements of spatial coherence. The model of a ballistic shockwave with peak pressure amplitude (P_{max}) in Pa and period of N-waved shockwave signal (O_T) in s is given using Whitham Equations 2.6 and 2.7 are as follows: (Stoughton, 1997).

$$P_{\max} = \frac{0.53\, P_0 \left({M_{\text{mach}}}^2 - 1\right)^{\frac{1}{8}} d}{h^{\frac{1}{4}}\, b^{\frac{3}{4}}} \tag{2.6}$$

$$O_T = \frac{1.82\, M_{\text{mach}}\, b^{\frac{1}{4}}\, d}{c\, h^{\frac{1}{4}}\, ({M_{\text{mach}}}^2 - 1)^{\frac{3}{8}}} \tag{2.7}$$

where P_0 is ambient pressure in Pa, c is the speed of sound in m/s, M_{mach} is the Mach number, h is the projectile length in meters, d is the diameter of the bullet in meters, and b is the miss distance from the trajectory in meters. The output of the shockwave model ($P_{\max}$) is pressure depending on time.

Furthermore, the sound pulse of shockwave signal lasts for about 200μs with an SPL higher than 140 dB and the center frequency of ballistic shockwave is between 1 kHz and 5 kHz (Stoughton, 1997). Whitham shockwave model is illustrated in Figure 2.8.

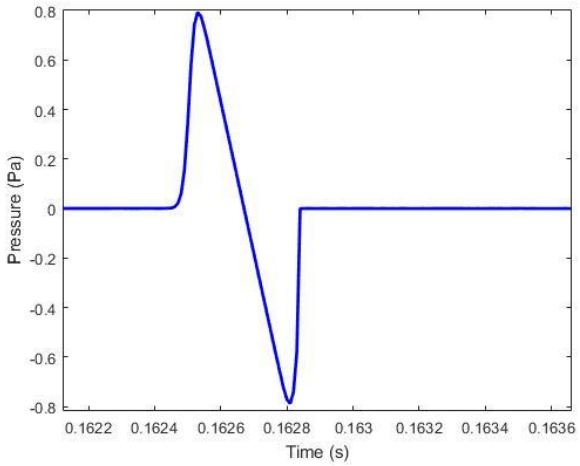

Figure 2.8: Whitham Shockwave Model

The values of the parameters presenting shockwave signal illustrated in Figure 2.8 are listed in Table 2.2.

Table 2.2. The Parameters of the Shockwave Signal

Parameter	Value
Ambient Pressure (P_0)	101 Pa
Sound Speed (c)	343 m/s
Bullet Speed (v)	705 m/s
Mach Number (M_{mach})	2.06
Miss Distance (b)	Random Variable
The diameter of the Bullet (d)	39 mm
Projectile Length (h)	7.62 mm
Center Frequency (f_c)	1 – 5 kHz
Sampling Frequency (f_s)	50 kHz

The values of bullet diameter and length are the representative value of AK-47's bullet which is very common (Penn et al., 2016).

2.3. Range, Azimuth and Miss Distance Calculation

To determine the shooter location randomly on a bounded region, the bounded region for the Cartesian coordinate system is introduced, firstly. The bounded region for the shooter location denoted by $\boldsymbol{X}$ matrix is as follows:

$$\boldsymbol{X} = \begin{bmatrix} 1000 & -1000 \\ 1000 & -1000 \end{bmatrix} \text{ in meters} \tag{2.8}$$

By using the random number generator, the target is located in a bounded region. The location vector $\boldsymbol{l}_s$ of the shooter is the following:

$$\boldsymbol{l}_{\mathrm{s}} = \begin{bmatrix} l_{\mathrm{x}} \\ l_{\mathrm{y}} \end{bmatrix} \tag{2.9}$$

After arranging all the location of the shooter into the bounded region, true values of range R in meters, and the azimuth of the shooter θ_{MB} in radians are calculated with the given formula 2.10 and 2.11:

$$R = \sqrt{{l_{\mathrm{x}}}^2 + {l_{\mathrm{y}}}^2} \tag{2.10}$$

$$\theta_{MB} = \arctan\left(\frac{l_{\mathrm{y}}}{l_{\mathrm{x}}}\right) \tag{2.11}$$

where l_{x} and l_{y} are the x and y coordinates of the shooter location in meters.

The miss distance (b) is the closest distance between the sensor array and the trajectory of the bullet. So, the vector of the sensor array and vector of the projectile trajectory are perpendicular to each other as shown in Figure 2.9.

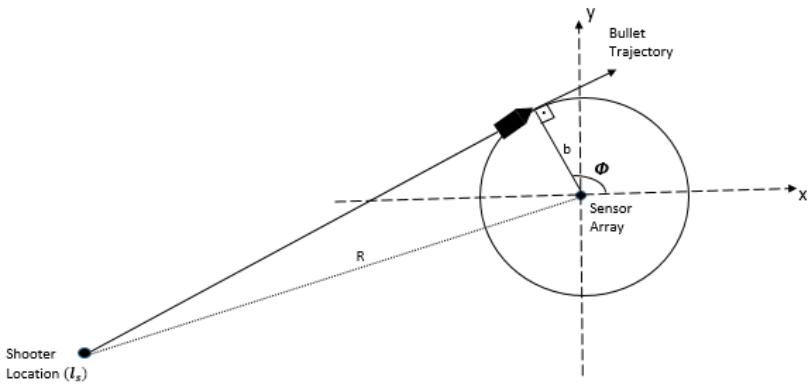

Figure 2.9: Miss Distance (b) Demonstration

The miss distance (b) is provided by the user or determined randomly to the simulation of the sniper localization system. The miss point $(b_{\mathrm{x}}, b_{\mathrm{y}})$ in the Cartesian coordinate, is calculated through Equations 2.12, 2.13, and 2.14.

$$b_{\mathrm{x}} = b\cos(\phi) \tag{2.12}$$

$$b_{\mathrm{y}} = b\sin(\phi) \tag{2.13}$$

where b is the miss distance in meters, ϕ is the angle of miss point in radians.

$$\hat{\phi} = \underset{\phi}{\operatorname{argmin}}\ b_{\mathrm{x}}\left(l_{\mathrm{x}} - b_{\mathrm{x}}\right) + b_{\mathrm{y}}\left(l_{\mathrm{y}} - b_{\mathrm{y}}\right) \tag{2.14}$$

where $\hat{\phi}$ is the estimate of the angle of miss point ϕ in radians and its value answers the miss distance, and x-y components of the miss distance b_{x} and b_{y} in meters are calculated through the Equations given above.

2.4. Line of Fire and Detach Point of Shockwave

To determine the line of fire, x-y coordinates of miss distance and x-y coordinates of shooter location that are calculated in Section 2.3 are necessary. While $\boldsymbol{s}_{\mathrm{LOF}}$ represents the starting point vector of the line of fire which is equal to the location vector of the shooter, $\boldsymbol{e}_{\mathrm{LOF}}$ provides with its endpoint vector which is the miss point vector.

$$\boldsymbol{s}_{\mathrm{LOF}} = \boldsymbol{l}_{\mathrm{s}} = \begin{bmatrix} l_{\mathrm{x}} \\ l_{\mathrm{y}} \end{bmatrix} \tag{2.15}$$

$$\boldsymbol{e}_{\mathrm{LOF}} = \begin{bmatrix} b_{\mathrm{x}} \\ b_{\mathrm{y}} \end{bmatrix} \tag{2.16}$$

$\boldsymbol{m}_{\mathrm{LOF}}$ represents the slope vector of the line of fire which is calculated through Equation 2.17.

$$\boldsymbol{m}_{\mathrm{LOF}} = \begin{bmatrix} m_{\mathrm{x}} \\ m_{\mathrm{y}} \end{bmatrix} = \begin{bmatrix} \cos\left(-\arctan\left(\dfrac{l_{\mathrm{y}} - b_{\mathrm{y}}}{l_{\mathrm{x}} - b_{\mathrm{x}}}\right)\right) \\ \sin\left(\arctan\left(\dfrac{l_{\mathrm{y}} - b_{\mathrm{y}}}{l_{\mathrm{x}} - b_{\mathrm{x}}}\right)\right) \end{bmatrix} \tag{2.17}$$

Although the shockwave moves through its trajectory with supersonic projectile, the acoustic signal of shockwave reaches the sensor array with sound speed. So, there is

a detachment point of the bullet to leave the acoustic signal of the shockwave from the bullet. Equation 2.18 to calculate the detachment point of the gun is as follows:

$$\hat{\mathrm{z}} = \underset{z}{\operatorname{argmin}} \frac{\sqrt{(l_{\mathrm{x}} - z\, m_{\mathrm{x}})^{\mathbf{2}} + \ (l_{\mathrm{y}} - z\, m_{\mathrm{y}})^{\mathbf{2}}}}{c} + \frac{z}{v} \tag{2.18}$$

where z is the distance between the detach point and the location of the shooter in meters, c is the bullet speed in m/s, m_{x} and m_{y} are the x and y coordinates of the line of fire vector in meters, l_{x} and l_{y} are the x and y coordinates of the shooter location in meters, v is the sound speed in m/s and $\hat{z}$ value is the estimate of the distance between the detachment point of the shockwave and the shooter location. The x-y coordinates of the detachment point vector $\boldsymbol{d}_{\mathrm{SW}}$ and the true azimuth angle of the shockwave θ_{SW} in radians are calculated using the Equation 2.19 and 2.20 below.

$$\boldsymbol{d}_{\mathrm{SW}} = \begin{bmatrix} d_{\mathrm{x}} \\ d_{\mathrm{y}} \end{bmatrix} = \begin{bmatrix} l_{\mathrm{x}} - \hat{\mathrm{z}}\, m_{\mathrm{x}} \\ l_{\mathrm{y}} - \hat{\mathrm{z}}\, m_{\mathrm{y}} \end{bmatrix} \tag{2.19}$$

$$\theta_{\mathrm{SW}} = \arctan\left(\frac{d_{\mathrm{y}}}{d_{\mathrm{x}}}\right) \tag{2.20}$$

where d_{x} and d_{y} are the x-y coordinates of detachment point in meters, and l_{x} and l_{y} are the x and y coordinates of the shooter location in meters.

2.5. Time of Arrival Calculation for Acoustic Events

The following formulas are used to find the time of arrival (TOA) of the muzzle blast and the shockwave signals for the geometrical model in s (Bedard et al., 2003):

$$t_{\mathrm{MB}} = \frac{R}{c} \tag{2.23}$$

where c is the sound speed in m/s, and R is the range of the shooter in meters.

$$t_{\mathrm{SW}} = \frac{z}{v} + \frac{b}{c\cos(\beta)} \tag{2.24}$$

where z is the distance between the shooter and the detach point in meters, b is the miss distance in meters, v is the bullet speed in m/s, and β is the shockwave opening angle called Mach angle in radians.

2.6. Transmission Loss Model

The definition of the transmission loss is the accumulated degradation in the waveform energy as the sound propagates outward from the source signal to the received sensor through the air. Moreover, when the sound propagates through its medium, conversion of acoustic energy into other types of energy as the consequence of making interaction with its medium causes the absorption loss which is the part of transmission loss (T_{loss}). Therefore, the summation of absorption loss (A_{loss}) and spreading loss (S_{loss}) as indicated in Equation 2.25.

$$T_{\text{loss}} = A_{\text{loss}} + S_{\text{loss}} \quad \text{in dB} \tag{2.25}$$

2.6.1. Absorption Loss Model

The model of absorption of sound in the atmosphere is dependent on the frequency of the signal, air temperature, humidity, and atmospheric pressure. Atmospheric absorption formulation is given in Equation 2.26 (Bass et al., 1990; Bass et al., 1995):

$$log_{10}\frac{P_{\text{sat}}}{P_{\text{s0}}} = 10.79586\left(1-\left(\frac{T_{01}}{T}\right)\right) - 5.02808\, log_{10}\left(\frac{T}{T_{01}}\right) \tag{2.26}$$

$$+1.50474\ \times 10^{-4}\left(1-10^{-8.29692\left(\frac{T_{01}}{T}-1\right)}\right) - 2.2195983$$

$$-4.2873\ \times\ 10^{-4}\left(1-10^{-4.76955\left(\frac{T_{01}}{T}-1\right)}\right)$$

where P_{sat} is the saturation vapor pressure in Pa, P_0 is the reference value of atmospheric pressure in Pa, T is the atmospheric temperature in K, T_0 is 293.15 K as

reference atmospheric temperature, and T_{01} is 273.16 K as triple-point isotherm temperature in Kelvin.

The formulas to calculate the percentage of the molar concentration of water vapor (h) is following (Bass et al., 1990):

$$h = \frac{h_{\mathrm{r}} \left(\frac{P_{\mathrm{sat}}}{P_{\mathrm{s0}}}\right)}{\frac{P_{\mathrm{s}}}{P_{\mathrm{s0}}}} \tag{2.27}$$

where P_{s0} is the ambient pressure in Pa, P_{s} is the atmospheric pressure in Pa, and h_{r} is the relative humidity in percent.

The formulas for the oxygen $f_{\mathrm{r,O}}$ and nitrogen $f_{\mathrm{r,N}}$ relaxation frequencies in Hz are given below as 2.28 and 2.29 (Bass et al., 1995):

$$f_{\mathrm{r,O}} = \frac{1}{P_{\mathrm{s0}}} \left(24 + 4.04 \times 10^{4} h \frac{0.02 + h}{0.391 + h}\right) \tag{2.28}$$

$$f_{\mathrm{r,N}} = \frac{1}{P_{\mathrm{s0}}} \left(\frac{T_0}{T}\right)^{\frac{1}{2}} \left(9 + 280 h e^{-4.17\left(\left(\frac{T_0}{T}\right)^{\frac{1}{3}} - 1\right)}\right) \tag{2.29}$$

The formula for the absorption loss of sound (A_{loss}) in the air in dB is given below (Bass et al., 1990):

$$A_{\mathrm{loss}} = 8.7\, R\, f^2 \left(1.84 \times 10^{-11} \left(\frac{P_{\mathrm{s}}}{P_{\mathrm{s0}}}\right)^{-1} \left(\frac{T}{T_0}\right)^{\frac{1}{2}} + \left(\frac{T}{T_0}\right)^{-\frac{5}{2}} \frac{1.278x10^{-2}\, e^{-\frac{2239.1}{T}}}{f_{\mathrm{r,O}} + \frac{f^2}{f_{\mathrm{r,O}}}} \right)$$

$$+ \frac{f^2 \times 1.068x10^{-1}\, e^{-\frac{3352}{T}}}{f_{\mathrm{r,N}} + \frac{f^2}{f_{\mathrm{r,N}}}} \quad [dB] \tag{2.30}$$

where f is the acoustic frequency in Hz, and R is the range of the shooter in meters.

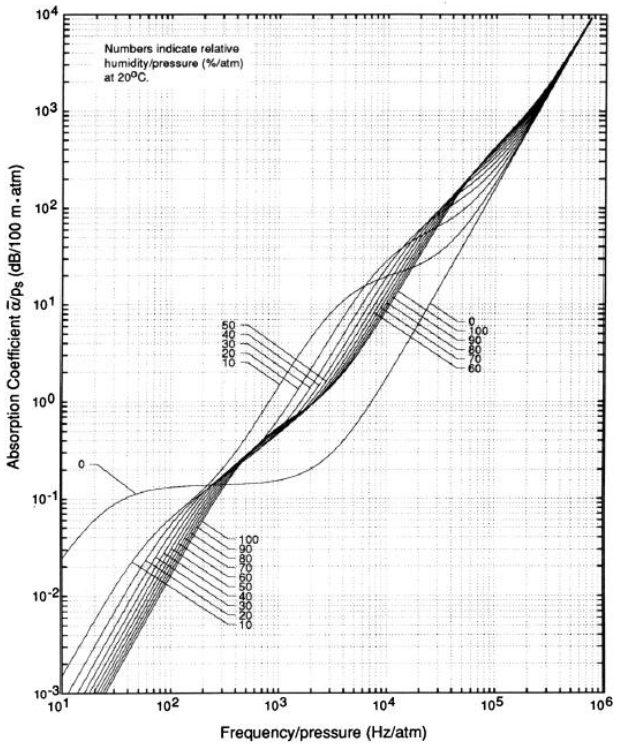

Figure 2.10: Sound Absorption Coefficient per Atmosphere (Bass et al., 1995)

Figure 2.10 illustrates the sound absorption coefficient per atmosphere pressure in terms of the frequency of the acoustic signals.

2.6.2. Spreading Loss Model

Spreading loss can be described as the loss due to the propagation of sound towards the sensor array. When the signal travels from the shooter location to the sensor array, the spreading loss occurs. Spreading loss is inversely proportional to the distance between the shooter location and the sensor array. The spreading loss formula (S_{loss}) is given below in Equation 2.31 (Roes et al., 2012).

$$S_{\text{loss}} = 20 \log\left(\sqrt{{l_{\text{x}}}^2 + {l_{\text{y}}}^2}\right) \text{ in dB} \tag{2.31}$$

where l_{x} and l_{y} are x and y coordinates of the shooter in meters, respectively.

2.7. Acoustic Signals with Additive White Gaussian Noise

Noisy data vector of muzzle blast signal $\boldsymbol{y}_{\mathrm{MB}}(t)$ can be described with Equation 2.32 (Oktel et al., 2005):

$$\boldsymbol{y}_{\mathrm{MB}}(t) = \boldsymbol{m}(\theta)\, s_{\mathrm{MB}}(t) + \boldsymbol{n}_{\mathrm{MB}}(t) \qquad \mathrm{t} = 1, 2, \ldots, \mathrm{N} \qquad (2.32)$$

where $\boldsymbol{m}(\theta)$ is $M \times 1$ array manifold vector given in Equation 2.34, $s_{\mathrm{MB}}(t)$ is the complex baseband signal representing the muzzle blast, $\boldsymbol{n}_{\mathrm{MB}}$ (t) is $M \times 1$ Gaussian noise vector with zero mean and covariance matrix $\sigma^2 \boldsymbol{I}_M$, M is the number of sensors, and N is the number of snapshots.

Noisy data vector of shockwave signal $\boldsymbol{y}_{\mathrm{SW}}(t)$ can be described with Equation 2.33 (Oktel et al., 2005):

$$\boldsymbol{y}_{\mathrm{SW}}(t) = \boldsymbol{m}(\theta)\, s_{\mathrm{SW}}(t) + \boldsymbol{n}_{\mathrm{SW}}(t) \qquad \mathrm{t} = 1, 2, \ldots, \mathrm{N} \qquad (2.33)$$

where $\boldsymbol{m}(\theta)$ is $M \times 1$ array manifold vector given in Equation 2.34, $s_{\mathrm{SW}}(t)$ is the complex baseband signal representing the shockwave, $\boldsymbol{n}_{\mathrm{SW}}$ (t) is $M \times 1$ Gaussian noise vector with zero mean and covariance matrix $\sigma^2 \boldsymbol{I}_M$, M is the number of sensors, and N is the number of snapshots.

The array manifold vector $\boldsymbol{m}(\theta)$ formulation (Dmochowski et al., 2007) is given below as Equation 2.34:

$$\boldsymbol{m}(\theta) = \begin{bmatrix} \exp\left(-j\frac{2\pi}{\lambda}\boldsymbol{p}_1^T\boldsymbol{u}(\theta)\right) \\ \exp\left(-j\frac{2\pi}{\lambda}\boldsymbol{p}_2^T\boldsymbol{u}(\theta)\right) \\ \vdots \\ \exp\left(-j\frac{2\pi}{\lambda}\boldsymbol{p}_M^T\boldsymbol{u}(\theta)\right) \end{bmatrix} \qquad (2.34)$$

where λ is the wavelength of the acoustic signals in meters, $\boldsymbol{p}_k$ is the position vector of k^{th} sensor consisting of x_k, and y_k which are the Cartesian coordinates in meters as

is given in Equation 2.2, and $\boldsymbol{u}(\theta)$ is the unit vector pointing at θ radians in azimuth, given as:

$$\boldsymbol{u}(\theta) = \begin{bmatrix} \cos(\theta) \\ \sin(\theta) \end{bmatrix}, \quad \theta \in [0, 2\pi) \tag{2.35}$$

2.8. Overview of Simulator

Acoustic sniper localization system simulator consists of modeling muzzle blast and shockwave signals, true range, and azimuth calculation, miss distance calculation, the line of fire, the detach point of the shockwave, time of arrival calculation for acoustic events, transmission loss model comprising absorption and spreading loss model and adding noise to the acoustic signals. There are two ways of using this simulator as depicted in Figure 2.11 and 2.12.

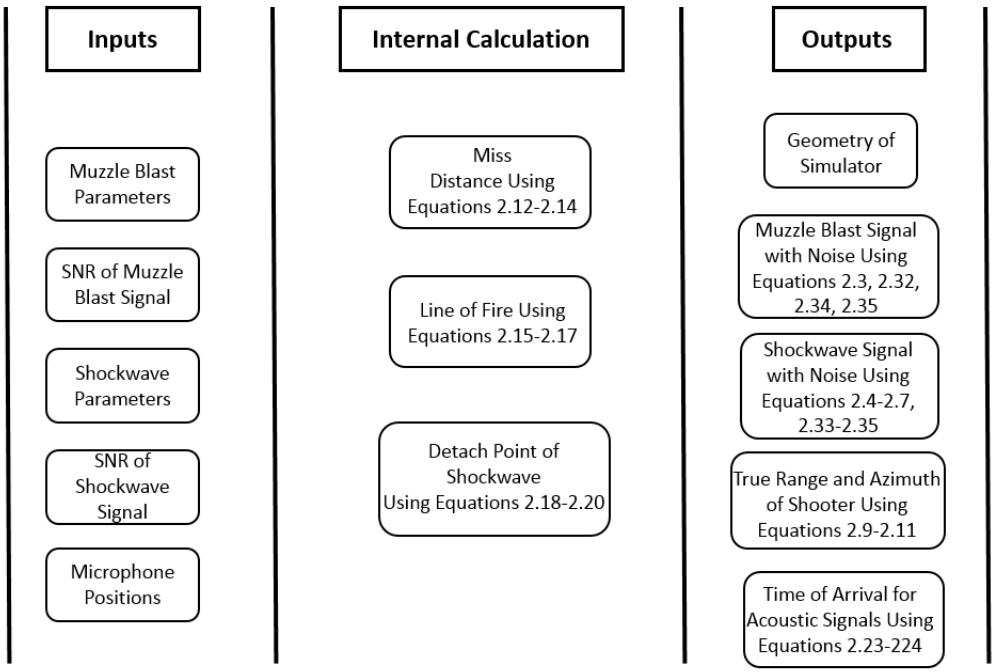

Figure 2.11: Overview of Simulator Version A

In the first version of the simulator as illustrated in Figure 2.11, muzzle blast and shock wave parameters, and desired SNR of muzzle blast and shockwave signals are the

inputs. By internal calculation of miss distance using Equations 2.12, 2.13, 2.14, line of fire using Equations 2.15, 2.16, 2.17, and detach point of shockwave using Equations 2.18, 2.19, 2.20, the simulator provides its geometry, muzzle blast and shock wave signals with desired SNR values using Equations 2.3, 2.4, 2.5, 2.6, 2.7, 2.32, 2.33, 2.34, and 2.35, true range and azimuth of the shooter using Equations 2.9, 2.10, 2.11 and TOA of acoustic events using Equations 2.23, 2.24 as an output.

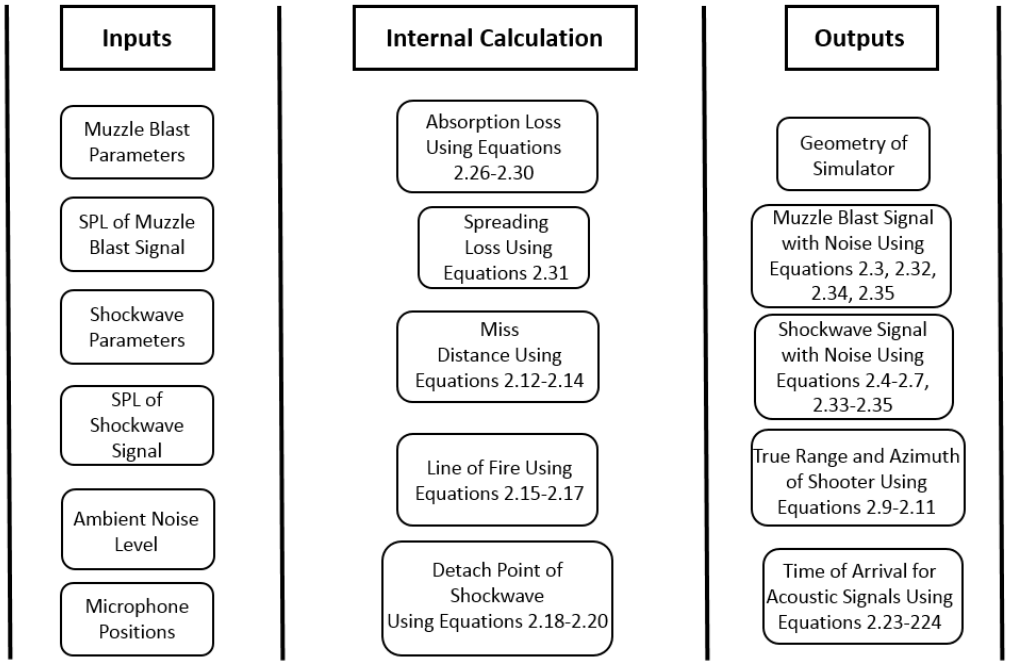

Figure 2.12: Overview of Simulator Version B

In the second version of the simulator as illustrated in Figure 2.12, muzzle blast and shock wave parameters, SPL of muzzle blast and shockwave signals, and ambient noise level are the inputs. By internal calculation of miss distance using Equations 2.12, 2.13, 2.14, line of fire using Equations 2.15, 2.16, 2.17 and detach point of shockwave using Equations 2.18, 2.19, 2.20, absorption, and spreading loss using 2.26, 2.27, 2.28, 2.29, 2.30, 2.31, the simulator provides its geometry, muzzle blast and shock wave signals with noise using 2.3, 2.4, 2.5, 2.6, 2.7, 2.32, 2.33, 2.34, and 2.35, true range and azimuth of shooter using Equations 2.9, 2.10, 2.11 and TOA of acoustic events using Equations 2.23, 2.24 as an output. SNR of muzzle blast and

shockwave signal is arranged in the light of absorption and spreading loss of the simulator in terms of the miss distance and the range of the shooter that are generated randomly.

Let's assume that the number of microphones is 4 and SNR of muzzle blast and shockwave signals are arranged as 10 dB, and 25 dB, respectively. Figure 2.13 gives an illustration of such a case with given SNR for uniform circular array (UCA).

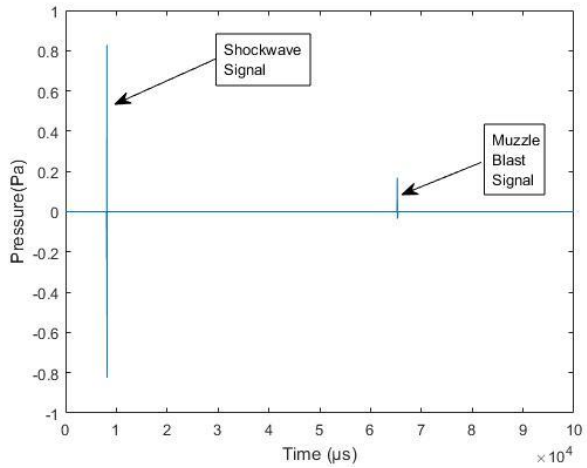

Figure 2.13: Simulator Data of Muzzle Blast and Shockwave Signals for UCA

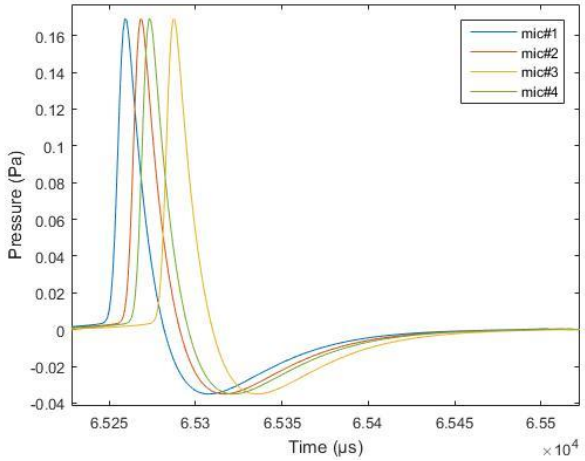

Figure 2.14: Simulator Data of Muzzle Blast Signal Received by Different Microphones of UCA

Figure 2.14 gives an example data of muzzle blast signal with 10 dB SNR for different sensors of UCA given in Figure 2.4. The number of microphones is 4 in Figure 2.14.

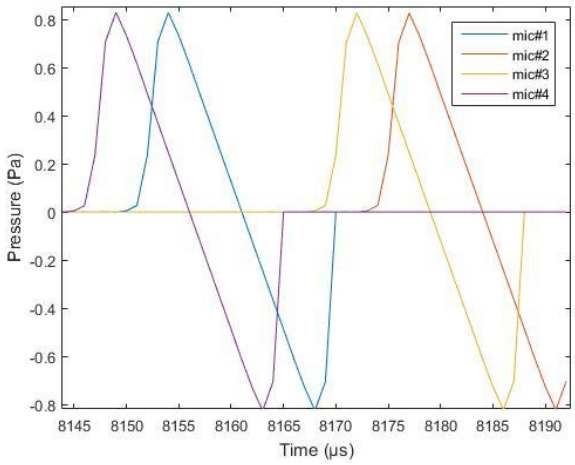

Figure 2.15: Simulator Data for Shockwave Signal Received by Different Microphones of UCA

Figure 2.15 gives an example data of shockwave signal with 25 dB SNR for different sensors of UCA given in Figure 2.4. The number of microphones is 4 in Figure 2.15. As it seen in Figure 2.13, there is a time delay between muzzle blast and shockwave signals since the bullet travels with supersonic speed which is quite larger than the sound speed. Also, there is a time delay between each microphone because of the distance difference between the shooter location and their positions. In Figure 2.13, 2.14, 2.15, the pressure values in Pa are calculated using Equation 2.1.

Both versions of the acoustic sniper localization system simulator will be used in Chapter 5 to determine detection zones for muzzle blast and shockwave signals.

CHAPTER 3

ESTIMATION FRAMEWORK

Having a wide dynamic range is an essential parameter of the sensor of the sniper localization system to capture both shockwave and muzzle blast signal. Although the bullet passes by the sniper localization system with a few meter distances away from it, the system is located at the top of a building and the distance between the projectile trajectory of the bullet and the location of the system is quite long, in some cases. Also, the distance between the sensor array and the shooter location might be quite high. Therefore, the weak acoustic signals can be captured to find DOA estimations. This problem imposes some constraints for the DOA algorithm to enhance signal power, so DAS beamforming technique (Benesty et al., 2007) to find DOA of both acoustic signatures as the muzzle blast and the shockwave. Moreover, how to use DOA estimation results of the DAS beamforming algorithm to calculate the range and the location of the shooter is provided.

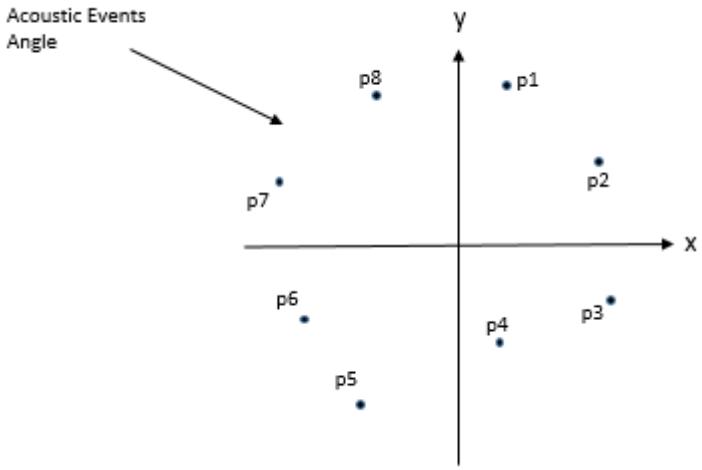

Figure 3.1: Two Dimensional Sensor Array Geometry and Acoustic Events on the Same Plane Region

The geometrical model of the sniper localization system outline with the azimuth angle of the shockwave (θ_{SW}) and the muzzle blast signals (θ_{MB}), range (R) and location of the shooter ($\boldsymbol{l}_{\mathrm{s}}$) is illustrated in Figure 3.2.

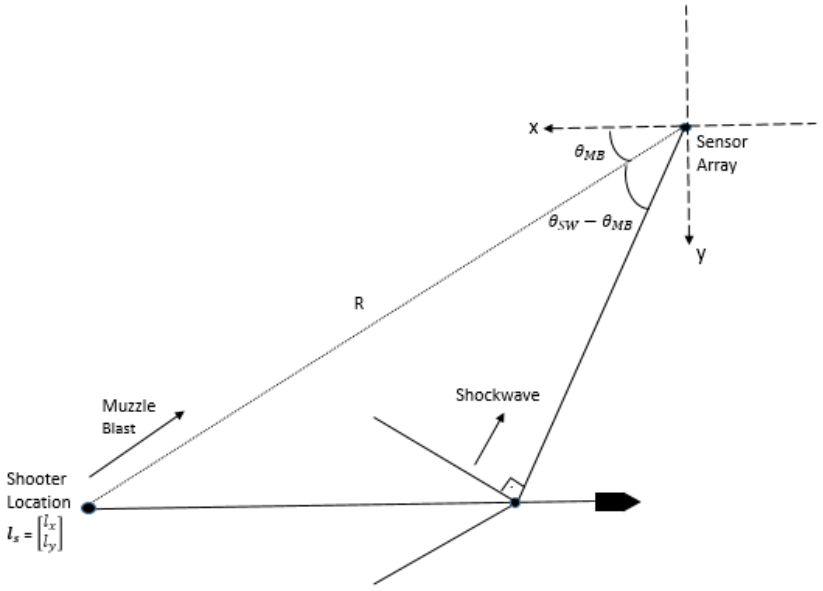

Figure 3.2: Geometrical Model of Estimation Framework

3.1. Direction of Arrival Estimation

The ballistic shockwave and muzzle blast are received by analog microphones and then converted to the digital signals for discrete-time delay and sum (DAS) beamformer (Warsitz et al., 2005) that runs into the embedded system architecture. The sampled complex baseband signal by an array of M sensors can be expressed as a given function:

$$\boldsymbol{y}[n] = \begin{bmatrix} y_1[n] \\ y_2[n] \\ \vdots \\ y_M[n] \end{bmatrix} \tag{3.1}$$

where M is the number of sensors, $y_k[n]$ is the complex baseband signal received by k^{th} sensor of the array.

Then, the sample covariance matrix $\widehat{\boldsymbol{R}}$ can be calculated in Equation 3.2. (Ramos et al., 2011)

$$\widehat{\boldsymbol{R}} = \frac{1}{N}\sum_{k=1}^{N} \boldsymbol{y}[n-k]\,\boldsymbol{y}^{H}[n-k] \tag{3.2}$$

where N is the number of snapshots.

Therefore, the DOA estimate ($\hat{\theta}$) can be obtained from Equation 3.3 (Ramos et al., 2011).

$$\hat{\theta} = \arg\max_{\theta}\left\{\boldsymbol{m}^{H}(\theta)\,\widehat{\boldsymbol{R}}\,\boldsymbol{m}(\theta)\right\} \tag{3.3}$$

where $\boldsymbol{m}(\theta)$ is the array manifold vector as it is given in Equation 2.34. By using Equations 3.1, 3.2, and 3.3, DOA estimation of muzzle blast $\hat{\theta}_{\mathrm{MB}}$ and ballistic shockwave $\hat{\theta}_{\mathrm{SW}}$ can be provided.

3.2. Range and Location of the Shooter Estimation

Figure 3.3 illustrates the range R and the shooter location.

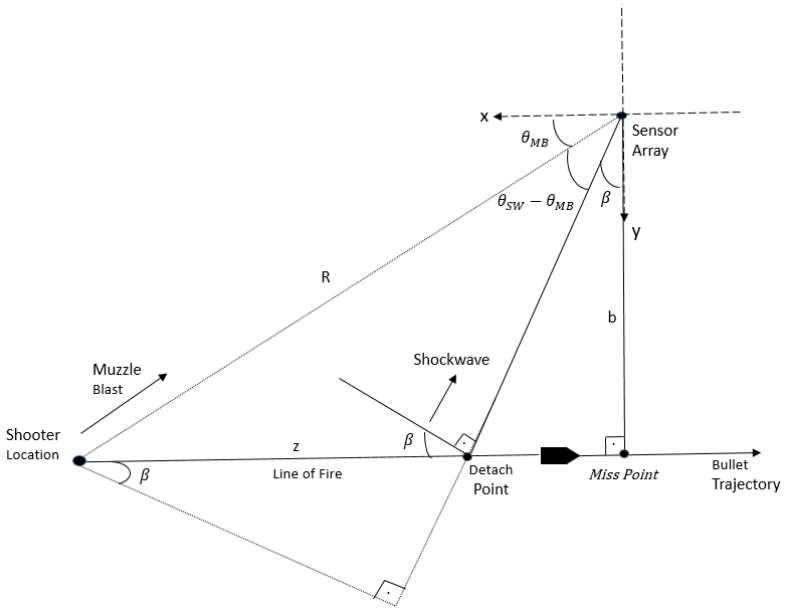

Figure 3.3: Range and Location Illustration of the Shooter

Two distinct acoustic signals are generated by the fire of small arms as shockwave and muzzle blast signals. The range is calculated by using the difference of velocities of shockwave and muzzle blast signals in the air. The difference between the arrival times of muzzle blast and shockwave signals is taken as the difference between the starting points of these signals. From the geometrical illustration given in Figure 3.3, Equation 3.6 can be formulated as follows:

$$R\ \cos(\theta_{\mathrm{MB}} - \theta_{\mathrm{SW}}) = z\sin(\beta)\ + \frac{b}{\cos(\beta)} \tag{3.6}$$

$$R - R\ \cos(\theta_{\mathrm{MB}} - \theta_{\mathrm{SW}})\ = R - \left(z\sin(\beta)\ + \frac{b}{\cos(\beta)}\right)$$

$$R\ (1 - \cos(\theta_{\mathrm{MB}} - \theta_{\mathrm{SW}})) =\ R - \left(z\sin(\beta)\ \ + \frac{b}{\cos(\beta)}\right)$$

where R is the range of the shooter in meters, z is the distance between the detach point and the shooter in meters, β is the Mach angle in radians, and b is the miss distance in meters.

By using Equations 2.23 and 2.24, time difference between muzzle blast and shockwave signals are calculated:

$$t_{\mathrm{MB}} - t_{\mathrm{SW}} = \frac{R}{c}\ - \left(\frac{z}{v} + \frac{b}{c\cos(\beta)}\right) \tag{3.7}$$

$$c(t_{\mathrm{MB}} - t_{\mathrm{SW}}) = R\ - c\left(\frac{z}{v} + \frac{b}{c\cos(\beta)}\right)$$

where R is the range of the shooter in m, z is the distance between detach point and shooter in m, β is the Mach angle in radians, b is the miss distance in meters, c is the sound speed in m/s, v is the bullet speed in m/s, t_{MB} is TOA of muzzle blast signal in s, and t_{SW} is TOA of shockwave signal in s.

Using Equation 2.4,

$$c\ (t_{\mathrm{MB}} - t_{\mathrm{SW}}) = R\ - \left(z\sin(\beta) + \frac{b}{\cos(\beta)}\right) \tag{3.8}$$

since Equations 3.6 and 3.8 are equal to each other, Equations 3.9 and 3.10 are used to find the estimate of the range ($\hat{R}$) and the estimate of the shooter location vector ($\hat{\boldsymbol{l}}_{\mathrm{s}}$) (Bedard et al., 2003).

$$\hat{R} = \frac{c\ (t_{\mathrm{MB}} - t_{\mathrm{SW}})}{1 - \cos\left(\hat{\theta}_{\mathrm{MB}} - \hat{\theta}_{\mathrm{SW}}\right)} \tag{3.9}$$

$$\hat{\boldsymbol{l}}_{\mathrm{s}} = \begin{bmatrix} l_x \\ l_y \end{bmatrix} = \begin{bmatrix} \hat{R}\cos\left(\hat{\theta}_{\mathrm{MB}}\right) \\ \hat{R}\sin\left(\hat{\theta}_{\mathrm{MB}}\right) \end{bmatrix} \tag{3.10}$$

where c is the sound speed in m/s, t_{MB} is the arrival time of muzzle blast in s, t_{SW} is the arrival time of shockwave signal in s, $\hat{\theta}_{\mathrm{MB}}$ is the estimate of the DOA for the muzzle blast in radians, and $\hat{\theta}_{\mathrm{SW}}$ is the estimate of the DOA for the shockwave signal in radians.

Figure 3.4 illustrates the result of the range formula given in Equation 3.9.

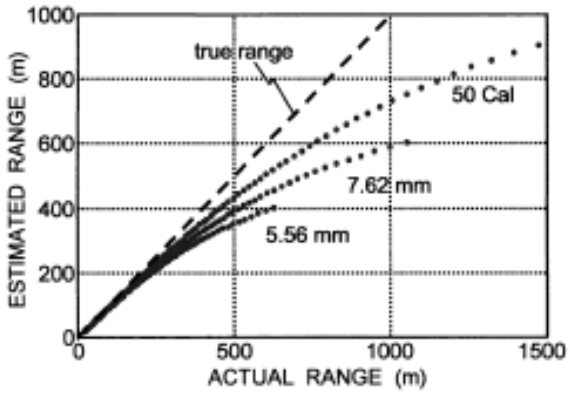

Figure 3.4: Range Estimation Using Equation 3.9

3.3. Overview of Estimation Framework

The estimation framework consists of DOA estimation for muzzle blast and shockwave signals, the range, and location of the shooter estimation. The model of estimation framework is depicted in Figure 3.5.

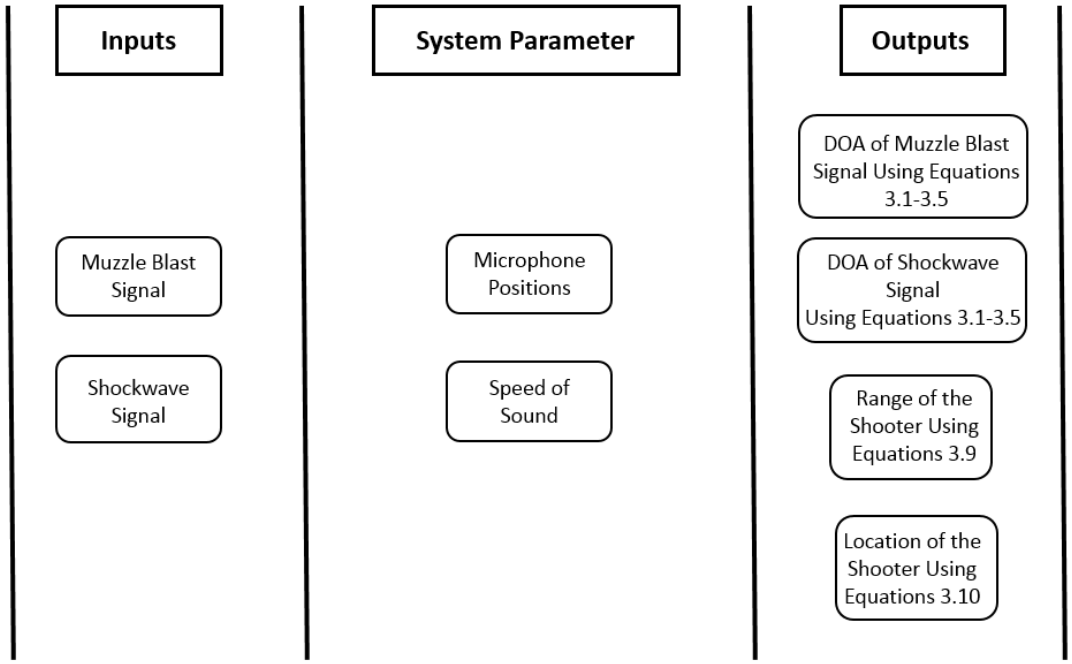

Figure 3.5: Estimation Framework Model

In the estimation framework model, muzzle blast and shockwave signals generated by acoustic sniper localization system simulator are the inputs. By using system parameter such as microphone positions, and speed of sound, DOA of muzzle blast and shockwave signals using 3.1-3.5, range of the shooter using Equation 3.9, and location of the shooter using Equation 3.10 are calculated.

Figure 3.6 illustrates the azimuth angle accuracy of the muzzle blast signal, in other words, the azimuth angle accuracy of the shooter performance comparison for different SNR values. The azimuth accuracy error for Pilarw and Ferret systems which are some of well-known acoustic sniper localization systems given in Table 1.1 is 2°.

However, there is no enough information in the datasheets of these systems about in which weather conditions and SNR values, these systems have 2° azimuth accuracy error. Therefore, the black line drawn in Figure 3.6 gives 2° representative azimuth accuracy error. The red line with '*' represents the azimuth accuracy error of UCA for different SNR of muzzle blast signal.

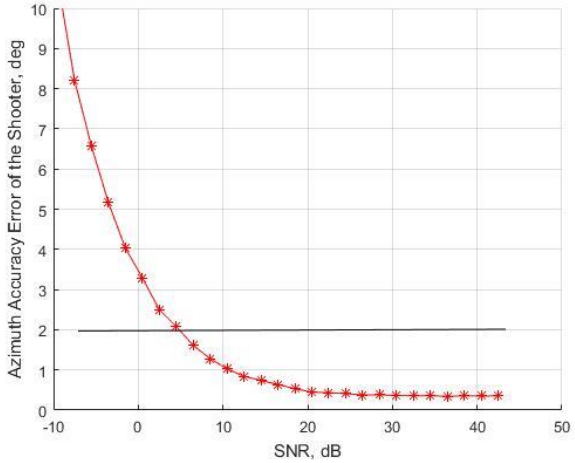

Figure 3.6: Azimuth Accuracy Error of the Shooter for UCA

In Figure 3.6, y-axis, which is mean error (ME^{θ}) of the azimuth accuracy in deg, is calculated through Equation 3.11.

$$ME^{\theta} = \frac{180^{\circ}}{K\pi}\sum_{n=1}^{K}\left|\hat{\theta}_n - \theta_n\right| \tag{3.11}$$

where $\hat{\theta}_n$ and θ_n are the estimated and true DOA for the deterministic muzzle blast signal model in radians, K is the Monte Carlo simulation number which is 1000. In each Monte Carlo iteration, the location of the shooter is chosen randomly as it is indicated in Equation 2.8. It means that the true azimuth angle of the shooter is uniformly distributed in the interval [0, 2π). The SNR of the shockwave signal is 25 dB which will be indicated in Section 5.2.

Figure 3.8 illustrates the range accuracy error of the shooter performance comparison for different SNR values. The range accuracy error for well-known acoustic sniper localization systems given in Table 1.1 is ±10%. However, there is no enough

information in the datasheets of these systems about in which weather conditions and SNR values, these systems have ±10% range accuracy error. Therefore, the black line drawn in Figure 3.6 gives 10% representative range accuracy error. The red line with '*' represents the range accuracy error of UCA for different SNR of muzzle blast signal.

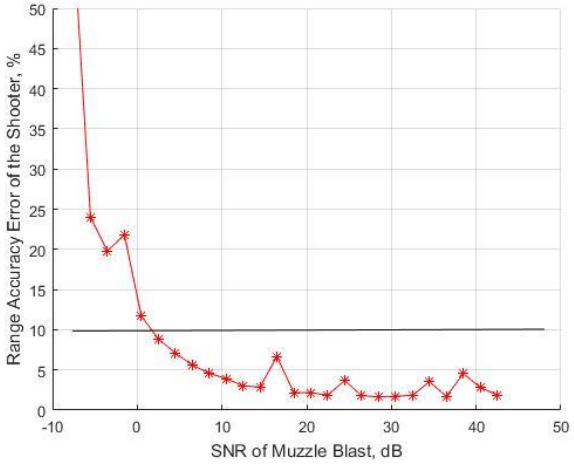

Figure 3.7: Range Accuracy Error of the Shooter for UCA

In Figure 3.7, y-axis, which is mean error (ME^R) of the range accuracy in percent, is calculated through Equation 3.12.

$$ME^R = \frac{100}{K}\sum_{n=1}^{K}\frac{|\hat{R}_n - R_n|}{R_n} \quad \text{in percent} \tag{3.12}$$

where $\hat{R}_n$ and R_n are the estimated and true range of the shooter, respectively. K is the Monte Carlo simulation number which is 1000. In each Monte Carlo iteration, the location of the shooter is chosen randomly as it is indicated in Equation 2.8. The SNR of the shockwave signal is 25 dB which will be indicated in Section 5.2.

CHAPTER 4

OPTIMIZATION AND GENETIC ALGORITHM

Optimization is regarded as a process to find the best solution to a problem by adjusting the inputs of the objective function of the problem to get the desired outputs. The objective function is a sample function of optimization used for finding the extreme points such as maximum or minimum over the determined search space. There are various approaches to solve optimization problems such as continuous optimization or discrete optimization, constrained optimization or unconstrained optimization, deterministic optimization or stochastic optimization and one or many objectives optimization (Andradóttir, 1998). In this thesis, the optimization of the sensor layout is based on the unconstrained and constrained optimization methods. If there are not any boundaries or specification for the search space of input variables, the optimization is called a constrained optimization method. However, the input variables of the search space do not have any restrictions or inequalities; the optimization is named unconstrained optimization method. Therefore, the difference between constraint and unconstrained optimization techniques is whether there is a constraint or not.

Likewise, the optimization methods can be categorized into two groups such as local and global optimizations relying on the search methods for the extreme points. Local optimization does not answer for finding the global optimum point since the global solution of the problem is not the priority for local optimization (Suh et al., 1987). As distinct from local optimization methods, global optimization finds the best solution to the objective function among all possible solutions over search space. One of the well-known global optimization techniques is genetic algorithm optimization which is a population-based method. In order to find the global minima of the objective function, this thesis concerns with the genetic algorithm.

4.1. Genetic Algorithm

The genetic algorithm (GA) is a wide spectrum of process derived from natural selection and genetics to find global optimum input variables to solve optimization problems. Apart from the classical algorithm which generates a single point in each step of the optimization, GA generates a population of points to solve its objective function which has nonlinearity, differentiability, or discontinuity. GA alternates the population of individuals to the fitness function, repeatedly. The individuals of the population are called chromosomes. At each iteration of GA process, the stream of computations is performed by evaluating the result of fitness function with chromosomes to determine the next generation. The chromosome that is fitted better to the fitness function is transplanted to the next generation to form the next population. It is named an elite chromosome. However, the other part of the individuals is changed by using some operations such as crossover and mutation, respectively until one of the stopping criteria is met (Vasconcelos et al., 2001). Figure 4.1 illustrates an example of the genetic algorithm process on MATLAB.

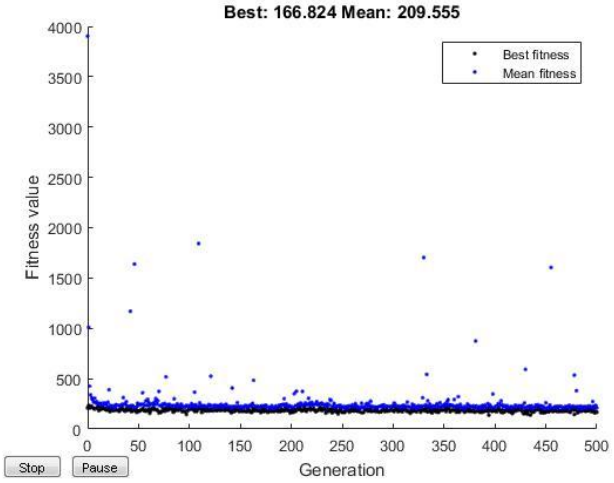

Figure 4.1: Genetic Algorithm Process on MATLAB

4.2. Chromosome and Population

The individuals that consist of a population are called chromosomes. The chromosomes can be regarded as a basic element of GA and solution to the objective

function. The dimension of the chromosome is the variable number of the objective function. In the optimization problem of this thesis, objective function has *2* x *M* variables where *M* is the number of sensors then the chromosome of GA is stated with Equation 4.1.

$$Chromosome = \begin{bmatrix} r_1 & r_2 & \dots & r_M \\ a_1 & a_2 & \dots & a_M \end{bmatrix} \quad (4.1)$$

where r_k and a_k are the radius and angle of each sensor over sample space in meters and radians, respectively. The detail of the sample space will be given in Chapter 5.

The population is a subset of candidate solutions to the objective function of the optimization problems. Besides, the population can be considered as a set of chromosomes. The first generation in an iterative process is called as initial population. Moreover, the size of the population is another parameter for the optimization problem. When its size increases, finding the best fitness value to the optimization problem becomes easier. However, increasing the size of the population causes more memory usage, cost and time (Arabas et al., 1994).

4.3. Creation of Next Population

After assigning the initial population or determining it randomly, the next population is arranged by using some chromosomes of the current population to avoid from loss of individuals that fits better to the objective function over their population. The chosen individuals are called as parents for the next generation and this choosing process is named selection. The rest of the chromosomes in the current population is used to involving in crossover and mutation processes. Crossover is a recombination of chromosomes from the current generation to create the next generation of the population. In some cases, the crossover does not enable the population to find the optimal variables for GA. In such a situation, mutation operation is used to provide optimization with genetic diversity from the current population. In mutation operation, some parts of the chromosomes are changed randomly to create genetic diversity. The

examples given in Figure 4.2 illustrate the selection, crossover and mutation operations (Konak et al., 2006).

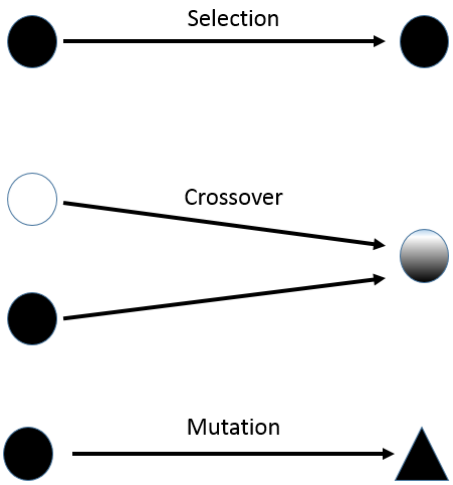

Figure 4.2: Operations of the Genetic Algorithm

4.4. Parameters of the Genetic Algorithm

After some iterations rounds that end up with the desired stopping criteria, GA reaches the best fitness value that is the smallest one. The stopping criteria and parameters of GA that are used in the optimization are given in Table 4.1:

Table 4.1. The Parameters of the Genetic Algorithm

Parameters of Genetic Algorithm	Statement
Generations	GA stops when it reaches to 500 since 500 generations is one of stopping criteria.
Time Limit	There is no time limit usage for the optimization given below sections
Function Tolerance	The algorithm trains until the average change in the fitness function value is less than function tolerance. It is 1e-6.
Constraint Tolerance	Constraint tolerance determines the feasibility of the optimization considering nonlinear constraints. It is 1e-3.
Population Size	Population size is the chromosome number in each population which is 50.

4.5. Flow Diagram of Genetic Algorithm

The flow diagram of the GA is depicted in Figure 4.3.

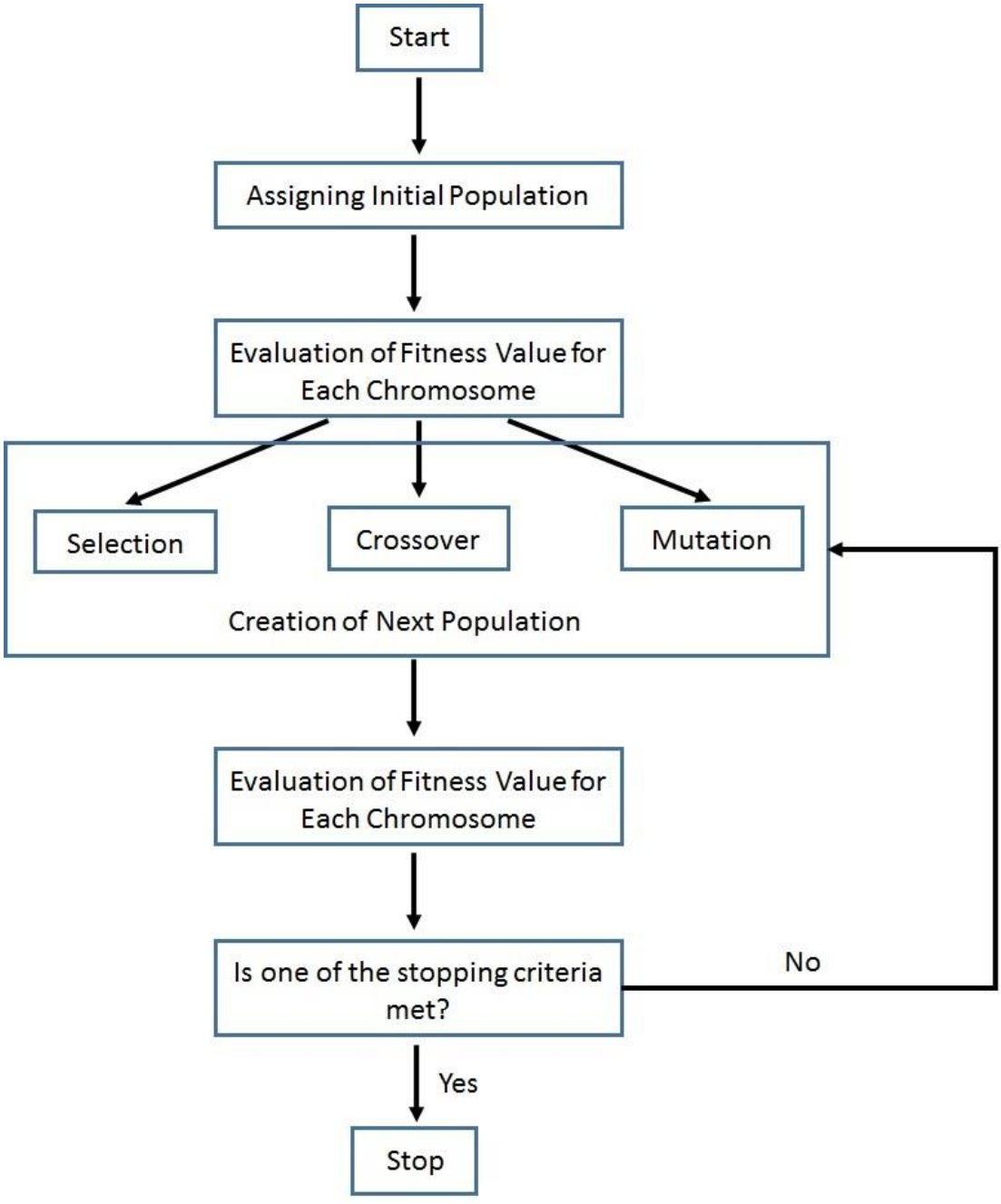

Figure 4.3: Flow Diagram of the Genetic Algorithm

CHAPTER 5

SENSOR LAYOUT OPTIMIZATION

Past studies generally focused on the optimization of weight vector for side lobe suppressing beamforming (He et al., 2015), and optimization based on DOA estimation (Birinci et al., 2007). However, this thesis examines the optimization of sensor layout based on shooter location estimation and side lobe suppression. Primarily, the detection zones of muzzle blast and shockwave signals are provided to determine optimization regions such as threshold or asymptotic regions. Then, the performance of UCA is given for a single DOA estimation which is the muzzle blast for different SNR values. After specifying the Monte-Carlo iteration number on the same sensor layout, the optimization techniques are applied based on shooter location estimation and side lobe suppression for the different number of sensors.

5.1. Specifying SNR Region for Muzzle Blast Signal

This section examines the SNR specifications for the muzzle blast signal. There exist many kinds of research focusing on DOA estimator optimization (Häcker et al., 2010). Figure 5.1 depicts different SNR region performance comparisons for maximum likelihood estimator with the CRLB of single DOA estimation (Fredrik, 2005).

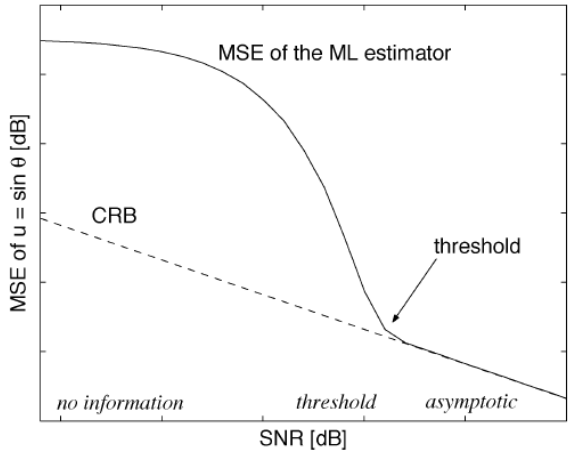

Figure 5.1: Different SNR Region Performance for Deterministic Signal Model in dB (Fredrik, 2005)

In Figure 5.1, there are three different regions such as no information, threshold and asymptotic region. Optimization is generally based on the threshold region since in no information region; there is a sudden increase below specific SNR values that cannot be attributed and optimization in the asymptotic region stands for local (Fredrik, 2005). Figure 5.2 depicts the different SNR region DOA estimation performance of deterministic muzzle blast signal for UCA array with $\lambda/2$ cm radius.

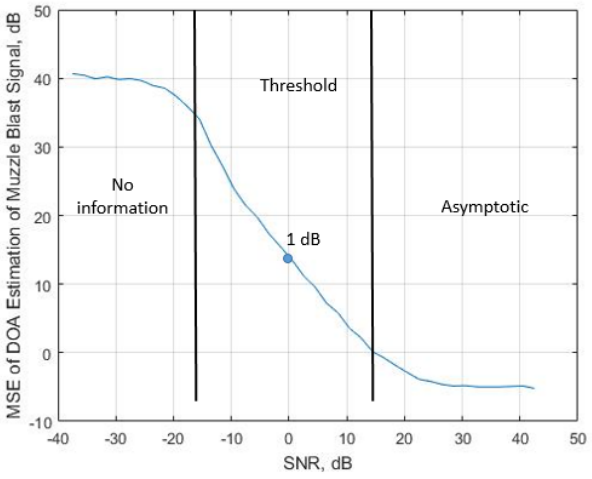

Figure 5.2: Different SNR Region Performance for Deterministic Muzzle Blast Signal in dB

In Figure 5.2, y-axis which is $MSE_{\mathrm{dB}}^{\theta}$ for the deterministic signal model is calculated through the given Equation 5.1.

$$MSE_{\mathrm{dB}}^{\theta} = 10\log\left(\frac{1}{K}\sum_{n=1}^{K}\left|\hat{\theta}_n - \theta_n\right|^2\right) \tag{5.1}$$

where $\hat{\theta}_n$ and θ_n are the estimated and true DOA for the deterministic muzzle blast signal model, *K* is Monte Carlo simulation number. In each Monte Carlo iteration, the location of the shooter is chosen randomly as it is indicated in Equation 2.8. The SPL of muzzle blast signal and shockwave signals are taken as constant whose value will be calculated in Section 5.2. It means that the true azimuth angle of the shooter is uniformly distributed in the interval [0, 2π).

As it is illustrated in Figure 5.2, the optimization is based on approximately between -15 dB and 17 dB SNR values. Therefore, the SNR of the muzzle blast to make optimization is chosen as 1 dB using Figure 5.2.

5.2. Detection Zones for Muzzle Blast and Shockwave

While the range of the shooter affects the SNR of the muzzle blast signal, the distance between the detach point of the shockwave and sensor influences the SNR of shockwave signal. Maximum Sound Pressure Level for muzzle blast and shockwave signals are considered as 130 dB and 140 dB respectively as it is given in Chapter 2, and let's assume that ambient noise level (S_{A}) is 60 dB which is the normal conversation dB level. By using the acoustic sniper localization system simulator version B described in Chapter 2, the maximum range of the shooter is calculated by Equation 5.2.

$$S_{\mathrm{MB}} - T_{\mathrm{loss}} - S_{\mathrm{A}} = 1dB \tag{5.2}$$

$$T_{\mathrm{loss}} = 130 - 1 - 60$$

where S_{MB} is the source level of the muzzle blast signal as 130 dB, T_{loss} is the transmission loss in dB, S_{A} is the ambient noise level in dB. Besides, $T_{\mathrm{loss}} = A_{\mathrm{loss}} + S_{\mathrm{loss}}$ where S_{loss} is the spreading loss in dB, and A_{loss} is the absorption loss in dB as it is given in Equation 2.25, and 1dB is the dB level which is proven in Section 5.1.

$$A_{\mathrm{loss}} + S_{\mathrm{loss}} = 69 \text{ dB} \tag{5.3}$$

$$20\log(R) + A_{\mathrm{loss}}(R, f, T, h_r) = 69$$

$$20\log(R) + A_{\mathrm{loss}}(R, 1000, 293, 50) = 69$$

$$20\log(R) + R \times 0.5/100 = 69$$

$$R = 1319 \text{ m}$$

where R is the range of the shooter in meters, f is the frequency of the signal in Hz, T is the air temperature in K, and h_r is the relative humidity in percent. Therefore, the maximum range of the shooter is calculated as 1319 m.

As it is given in Table 1.1 and 1.2, the maximum bullet detection range for similar systems is 200m. By using the acoustic sniper localization system simulator version B described in Chapter 2, SNR of the shockwave signal for the maximum bullet detection distance (S_{mbd}) in dB is calculated with Equation 5.4.

$$S_{\mathrm{SW}} - T_{\mathrm{loss}} - S_A = S_{\mathrm{mbd}} \tag{5.4}$$

$$140 - T_{\mathrm{loss}} - 60 = S_{\mathrm{mbd}}$$

where S_{SW} is source level of shockwave signal as 140 dB, S_A is the ambient noise level in dB, and $T_{\mathrm{loss}} = A_{\mathrm{loss}} + S_{\mathrm{loss}}$ as given in Equation 2.25,

$$80 - (A_{\mathrm{loss}} + S_{\mathrm{loss}}) = S_{\mathrm{mbd}} \tag{5.5}$$

$$20\log(y) + A_{\mathrm{loss}}(y_{mbd}, f, T, h_r) + 80 = S_{\mathrm{mbd}}$$

$$20\log(200) + A_{\mathrm{loss}}(200, 5000, 293, 50) = S_{\mathrm{mbd}}$$

$$80 - (46 + 8.8) = 25.2\ dB$$

where S_{mbd} is the SNR of the shockwave signal for the maximum bullet detection distance in dB, y_{mbd} is the maximum bullet detection distance in meters, f is the frequency of the signal in Hz, T is the air temperature in K, and h_r is the relative humidity in percent. Therefore, SPL of the shockwave signals for the maximum bullet detection range S_{mbd} which is taken as 200 m is calculated in Equation 5.5 as 25.2 dB. Detection zones of the muzzle blast and the shockwave signals are depicted in Figure 5.3.

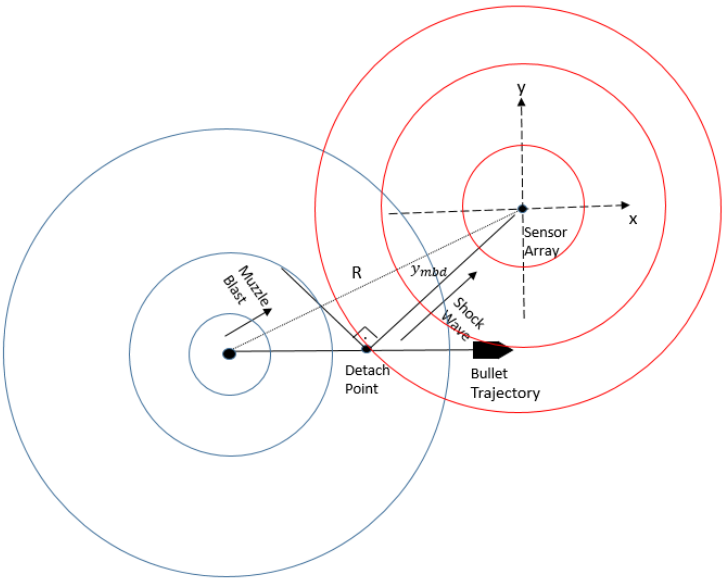

Figure 5.3: Detection Zones for Muzzle Blast and Shockwave

5.3. Specifying Monte Carlo Iteration Number

Figure 5.4 illustrates the performance comparison different MC simulation numbers such as 100 MC represented by blue, 1000 MC represented by red, and 5000 MC represented by green. Since 1000 MC results are very similar to 5000 MC, the optimizations and simulation results will be based on 1000 MC simulations. The y-axis of Figure 5.4 is calculated using Equation 5.1. However, x-axis of Figure 5.4 is the SNR of the muzzle blast signal in dB.

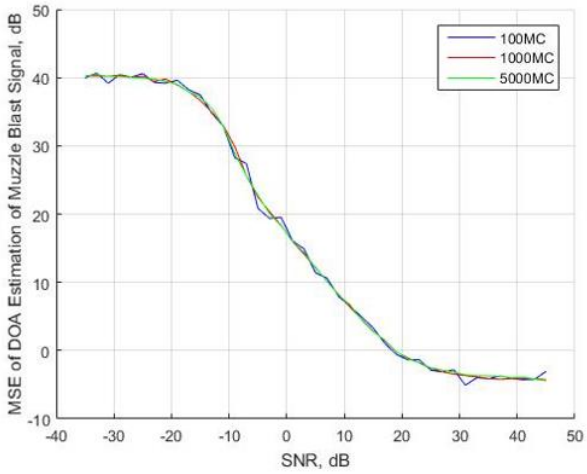

Figure 5.4: Comparison of Different Monte Carlo (MC) Simulation Number in dB

5.4. Sensor Layout Optimization Based on Side Lobe Suppression

In most applications of array signal processing, the main aim is to design an array that increases the accuracy of the DOA estimation of the received signal. However, there are some other criteria as side lobe suppression (SLS) that is related to the directivity and half-power beamwidth which is the different interpretation of CRB. Illustration of side-lobe suppression level (SLSL) and half-power beamwidth (HPB) is given in Figure 5.5 and 5.6, respectively.

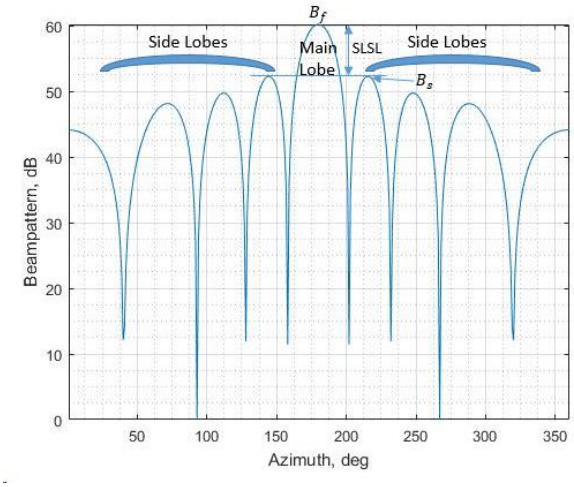

Figure 5.5: SLSL Example

As it is depicted in Figure 5.5, the lobe that has a maximum signal strength in the incident wave angle is called the main lobe and other lobes are called the side lobes. Side lobe suppression level (SLSL) is the difference between the peak of the main beam (B_f) and the peak of the highest side lobe (B_s) in dB.

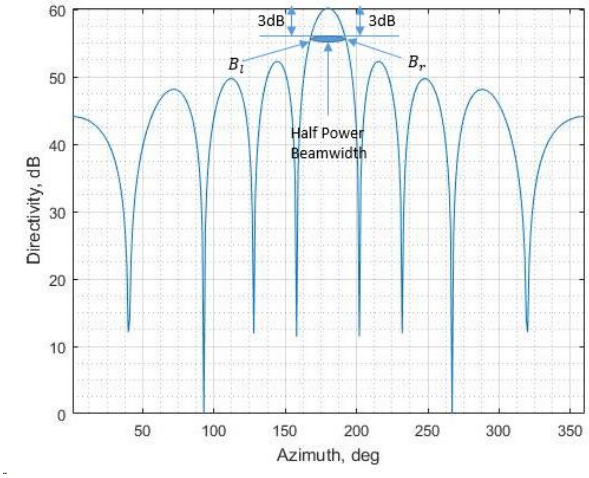

Figure 5.6: HPB Example

Besides, half-power beamwidth refers to the angle between the half-power points (B_l&B_r) of the main lobe. Half-Power points are the angles that have 3-dB less magnitude than the maximum of the beam pattern. Therefore, SLSL B_{SLSL} and HPB B_{HPB} are calculated through Equations 5.6 and 5.7

$$B_{\mathrm{SLSL}} = B_f - B_s \tag{5.6}$$

$$B_{\mathrm{HPB}} = B_l + B_r \tag{5.7}$$

In this part of the thesis, the optimization will be applied for side lobe suppression level by two different approaches as SLSL optimization without HPB constraint and SLSL optimization with HPB constraint. The optimizations are solved considering the worst-case optimization approach. Beamformer power vector ($\boldsymbol{g}$) is calculated through the array manifold vector $\mathbf{w}(\psi)$ as given in Equation 5.9 and weight matrix ($\boldsymbol{A}$) given in Equation 5.10.

$$\boldsymbol{g} = 20\, log|\boldsymbol{A}^H \boldsymbol{w}| = [B_1\ B_2\ \ldots\ B_N]^{\boldsymbol{T}} \tag{5.8}$$

where B_k is the beamformer power value corresponding to k^{th} beam angle.

The weight vector $\boldsymbol{w}(\psi)$ and the weight matrix $\boldsymbol{A}$ calculation (Dmochowski et al., 2007) are given in Equation 5.9, and 5.10.

$$\boldsymbol{w}(\psi) = \begin{bmatrix} \exp\left(-j\frac{2\pi}{\lambda}\,\boldsymbol{p}_1^T\,\boldsymbol{s}(\psi)\right) \\ \exp\left(-j\frac{2\pi}{\lambda}\,\boldsymbol{p}_2^T\,\boldsymbol{s}(\psi)\right) \\ \vdots \\ \exp\left(-j\frac{2\pi}{\lambda}\,\boldsymbol{p}_M^T\,\boldsymbol{s}(\psi)\right) \end{bmatrix} \tag{5.9}$$

$$\boldsymbol{A} = [\ \boldsymbol{w}(\psi_1), \boldsymbol{w}(\psi_2),\ \ldots\quad \boldsymbol{w}(\psi_N)\ ],\quad \psi \in [0, 2\pi) \tag{5.10}$$

where λ is the wavelength of the acoustic signal in meters, $\boldsymbol{p}_k$ is the position vector of k^{th} sensor consisting of x_k, and y_k which are the Cartesian coordinates in meters as is given in Equation 2.2, and $\boldsymbol{s}(\psi)$ is the steering vector pointing at ψ radians in azimuth, given as:

$$\boldsymbol{s}(\psi) = \begin{bmatrix} \cos(\psi) \\ \sin(\psi) \end{bmatrix},\ \psi \in [0, 2\pi) \tag{5.10}$$

5.4.1. SLSL Optimization without HPB Constraint

In SLSL optimization without HPB constraint section, the sensors of the microphone array are allowed to locate inside the circle with radius λ_{MB} and outside the circle with radius $\lambda_{\text{MB}}/2$, so it is not allowed to locate inside the circle with radius $\lambda_{\text{MB}}/2$ and outside the circle with radius λ_{MB}. The sensor location matrix given in Equation 2.2 is transformed into the spherical coordinate system with Equation 5.11.

$$\boldsymbol{B} = \begin{bmatrix} x_1 & x_2 & \ldots & x_M \\ y_1 & y_2 & \ldots & y_M \end{bmatrix} = \begin{bmatrix} r_1\cos(a_1) & r_2\cos(a_2) & \ldots & r_M\cos(a_M) \\ r_1\sin(a_1) & r_2\sin(a_2) & \ldots & r_M\sin(a_M) \end{bmatrix} \tag{5.11}$$

$$\boldsymbol{r} = \begin{bmatrix} r_1 \\ r_2 \\ \vdots \\ r_M \end{bmatrix} \text{ and } \boldsymbol{a} = \begin{bmatrix} a_1 \\ a_2 \\ \vdots \\ a_M \end{bmatrix} \tag{5.12}$$

where $\boldsymbol{r}$ in meters and $\boldsymbol{a}$ in radians are the radius and angle vector of sensor array given in Equation 5.12, respectively. The objective function for the SLSL optimization without HPB constraint is given in Equation 5.13.

$$\begin{aligned} &\max_{\boldsymbol{r},\boldsymbol{a}} \min(B_{\mathrm{SLSL}}^{\psi}) \\ &s.t. \frac{\lambda_{\mathrm{MB}}}{2} < r_k < \lambda_{\mathrm{MB}}, k = 1, \dots, M \\ &(k-1)\frac{2\pi}{M} < a_k < k\,\frac{2\pi}{M}\,, k = 1, \dots, M \end{aligned} \tag{5.13}$$

where B_{SLSL}^{ψ} is the side lobe suppression level in ψ-incident angle, r_i and a_i are the radius and angle concerning x-axis of the k^{th} sensor. λ_{MB} is the wavelength of the muzzle blast signal which is approximately 68 cm, M is the number of sensors. As it is indicated in the constraint part of the optimization formula, each sensor has $\frac{2\pi}{M}$ angle interval and $\lambda_{\mathrm{MB}}/2$ radius interval. The optimization is made for the different number of sensors (M) such as 4, 8 and 12 microphones.

5.4.1.1. Optimization of 4 Sensors

SLSL optimization without HPB constraint is made for 4 sensors using Equation 5.13, firstly. The sensor locations of GA and UCA are depicted in Figure 5.7.

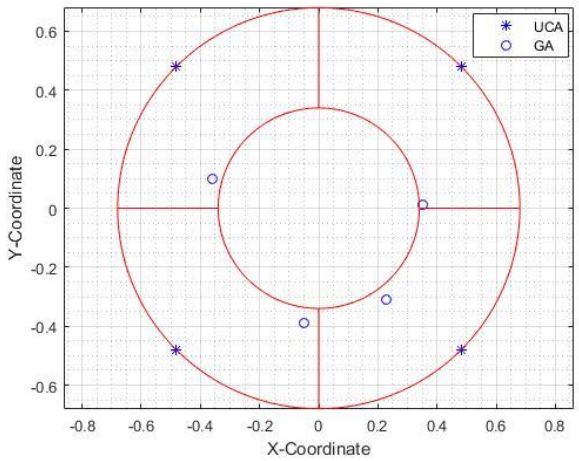

Figure 5.7: Sensor Location Demonstration of GA Based on SLSL without HPB Constraint and UCA for 4 Sensors in meters

In Figure 5.7, sensor locations of the GA and UCA are indicated with ‘o’ and ‘*’ blue colored symbols, respectively. The red lines show the restricted borders of each sensor. The sensor locations demonstrated in Figure 5.7 are given in Table 5.1.

Table 5.1: The Sensor Locations of GA Based on SLSL without HPB Constraint and UCA for 4 Sensors

Array Type	Radius Vector($\boldsymbol{r}$), meters	Angle Vector($\boldsymbol{a}$), radians
UCA	$\lambda_{\mathrm{MB}}[1\ 1\ 1\ 1]^T$	$\frac{\pi}{180°}[45°\ 135°\ 225°\ 315°]^T$
GA	$\lambda_{\mathrm{MB}}[0.52\ 0.55\ 0.58\ 0.57]^T$	$\frac{\pi}{180°}[2°\ 164°\ 263°\ 306°]^T$

The minimum SLSL and maximum HPB for the GA and UCA concerning the incident azimuth angle are illustrated in Figure 5.8.

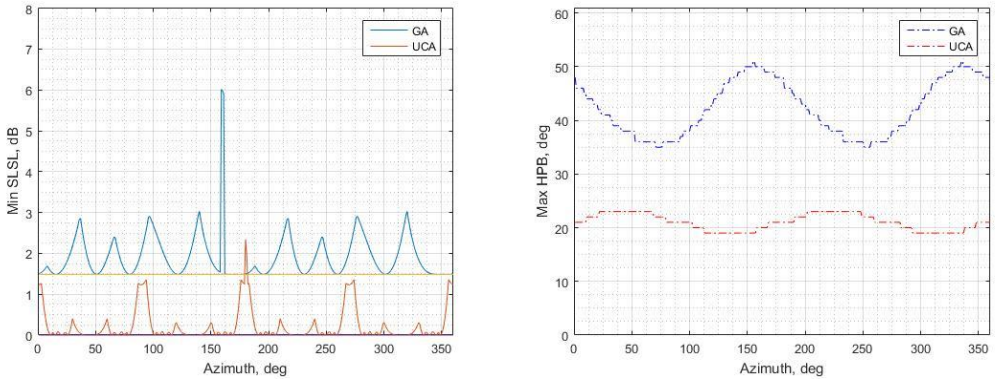

Figure 5.8: Minimum SLSL and Maximum HPB of GA Based on SLSL without HPB Constraint and UCA for 4 Sensors

Figure 5.8 shows that while there is no side lobe suppression for UCA, minimum SLSL is 1.48 dB for the sensor layout of GA based on SLSL without HPB constraint for 4 sensors. Besides, HPB of the sensor array of GA and UCA are 51° and 21°. Therefore, while the genetic algorithm suppresses the side lobe levels, the half-power beamwidth of the sensor array increases. The reason behind increasing HPB is the decrease in the aperture of the sensor array as it is illustrated in Figure 5.7.

Figure 5.9 depicts that the location estimation performance comparison of the sensor layouts given in Figure 5.7 using the acoustic sniper localization system simulator.

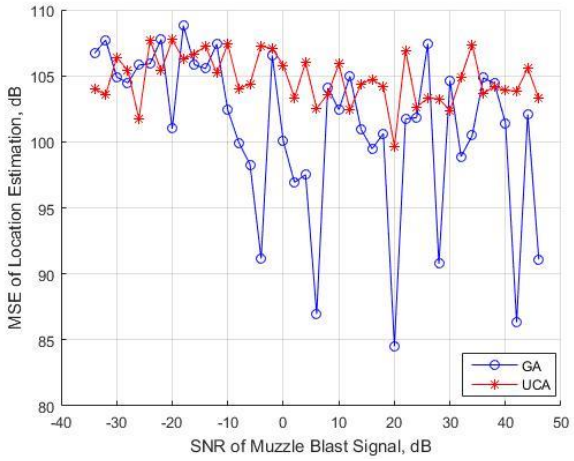

Figure 5.9: Location Estimation Performance Comparison of GA Based on SLSL without HPB Constraint and UCA for 4 Sensors in dB

In Figure 5.9, y-axis which is $MSE_{\mathrm{dB}}^{\boldsymbol{l}}$ for the shooter location estimation is calculated through the Equation 5.14.

$$MSE_{\mathrm{dB}}^{\boldsymbol{l}} = 10\log\left(\frac{1}{K}\sum_{n=1}^{K}\left\|\hat{\boldsymbol{l}}_n - \boldsymbol{l}_n\right\|^2\right) \tag{5.14}$$

where $\hat{\boldsymbol{l}}_n$ and $\boldsymbol{l}_n$ are the estimated and true location vector of the shooter, $\|.\|$ represents the L-2 norm operator, K is the Monte Carlo simulation number. In each Monte Carlo iteration, the location of the shooter is chosen randomly as it is indicated in Equation 2.8. The SPL of the muzzle blast signal and shockwave signals are taken as constant whose value will be calculated in Section 5.2. Therefore, true azimuth angle of the shooter is uniformly distributed in the interval [0, 2π).

Figure 5.9 illustrates that there is no significant performance difference between two arrays since the sensor layout of GA increases the minimum SLSL by only 1.48 dB, and the increase in the maximum HPB affects location estimation performance, negatively. Although the location estimation performance for the sensor layout of GA

seems better, the estimation regions are not enough recognizable as threshold region and asymptotic regions while SNR increases. Therefore, they are the expected results.

5.4.1.2. Optimization of 8 Sensors

SLSL optimization without HPB constraint is made for 8 sensors using Equation 5.13, secondly. The sensor locations of GA and UCA are depicted in Figure 5.9.

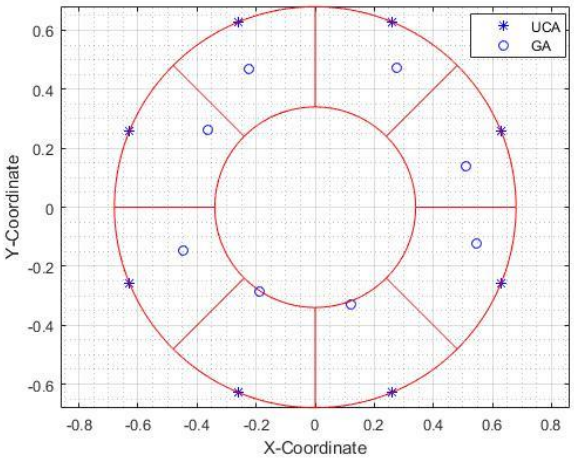

Figure 5.10: Sensor Location Demonstration of GA Based on SLSL without HPB Constraint and UCA for 8 Sensors in meters

In Figure 5.10, sensor locations of the GA and UCA are indicated with 'o' and '*' blue colored symbols, respectively. The red lines show the restricted borders of each sensor. The sensor locations demonstrated in Figure 5.10 are given in Table 5.2.

Table 5.2: The Sensor Locations of GA Based on SLSL without HPB Constraint and UCA for 8 Sensors

Array Type	Radius Vector($\boldsymbol{r}$), meters	Angle Vector($\boldsymbol{a}$), radians
UCA	$\lambda_{\mathrm{MB}}[1\ 1 \ldots 1\ ]^T$	$\frac{\pi}{180°}[23°\ 68°\ \ldots\ 338°]^T$
GA	$\lambda_{\mathrm{MB}}[0.78\ 0.8\ 0.77\ 0.66\ 0.69\ 0.51\ 0.52\ 0.82]^T$	$\frac{\pi}{180°}[2°\ 164°\ 263°\ 306°]^T$

The minimum SLSL and maximum HPB for the GA and UCA concerning the incident azimuth angle are illustrated in Figure 5.11.

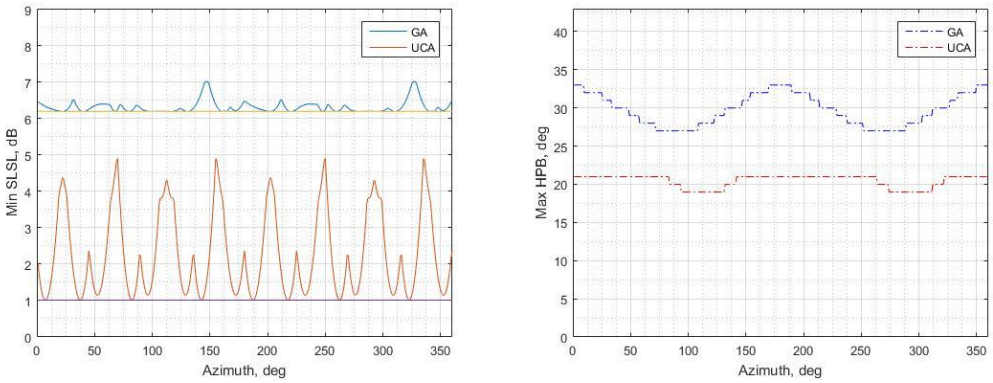

Figure 5.11: Minimum SLSL and Maximum HPB of GA Based on SLSL without HPB Constraint and UCA for 8 Sensors

Figure 5.11 shows that while the minimum SLSL of UCA is 1.11 dB, it is 6.2 dB for the sensor layout of GA based on SLSL without HPB constraint for 8 sensors. Besides, HPB of the sensor array of GA and UCA are 33° and 21°. Therefore, while the genetic algorithm suppresses the side lobe levels, the half-power beamwidth of the sensor array increases. The reason behind increasing HPB is the decrease in the aperture of the sensor array as it is illustrated in Figure 5.10.

Figure 5.12 depicts that the location estimation performance comparison of the sensor layouts given in Figure 5.10 using the simulator. Figure 5.12 illustrates that the location estimation performance of the sensor layout of the GA exceeds the performance of UCA. At the SNR values which are lower than 0 dB, there is no significant difference between two sensor arrays. However, especially in the asymptotic region, the performance of the optimized sensor layout is much better since the minimum SLSL of the optimized sensor layout is 5.1 dB more than the minimum SLSL of the UCA with the same radius. Although the HPB of the optimized sensor layout is quite larger, side lobe suppression seems to be more dominant. In Figure 5.12, y-axis which is $MSE_{\mathrm{dB}}^{\boldsymbol{l}}$ for the shooter location estimation is calculated through the Equation 5.14.

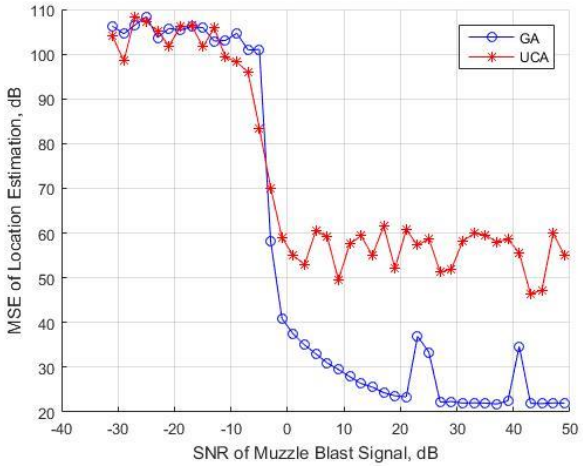

Figure 5.12: Location Estimation Performance Comparison of GA Based on SLSL without HPB Constraint and UCA for 8 Sensors in dB

5.4.1.3. Optimization of 12 Sensors

SLSL optimization without HPB constraint is made for 12 sensors using Equation 5.13, lastly. The sensor locations of GA and UCA are depicted in Figure 5.13.

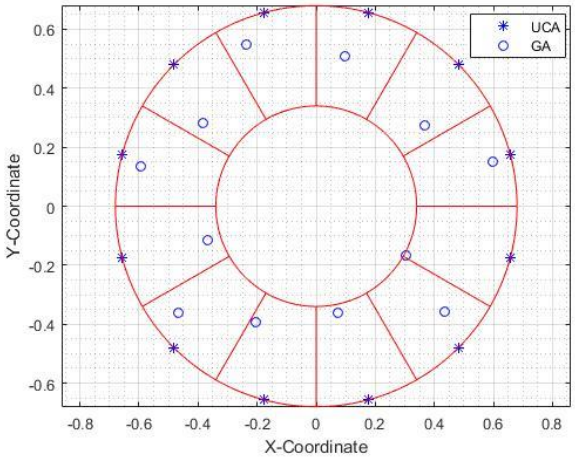

Figure 5.13: Sensor Location Demonstration of GA Based on SLSL without HPB Constraint and UCA for 12 Sensors in meters

In Figure 5.13, sensor locations of the GA and UCA are indicated with ‘o’ and ‘*’ blue colored symbols, respectively. The red lines show the restricted borders of each sensor. The sensor locations demonstrated in Figure 5.13 are given in Table 5.3.

Table 5.3: The Sensor Locations of GA Based on SLSL without HPB Constraint and UCA for 12 Sensors

Array Type	Radius Vector($\boldsymbol{r}$), meters	Angle Vector($\boldsymbol{a}$), radians
UCA	$\lambda_{\mathrm{MB}}[1\ 1 \ldots 1\ ]^T$	$\frac{\pi}{180°}[15°\ 45°\ \ldots\ 345°]^T$
GA	$\lambda_{\mathrm{MB}}[0.91\ 0.67\ .0.76\ 0.88\ 0.7\ 0.9\ 0.57\ 0.87\ 0.65\ 0.54\ 0.83\ 0.51]^T$	$\frac{\pi}{180°}[14°\ 36°\ 79°\ 113°\ 144°\ 167°\ 197°\ 218°\ 243°\ 282°\ 321°\ 331°]^T$

The minimum SLSL and maximum HPB for the GA and UCA concerning the incident azimuth angle are illustrated in Figure 5.14.

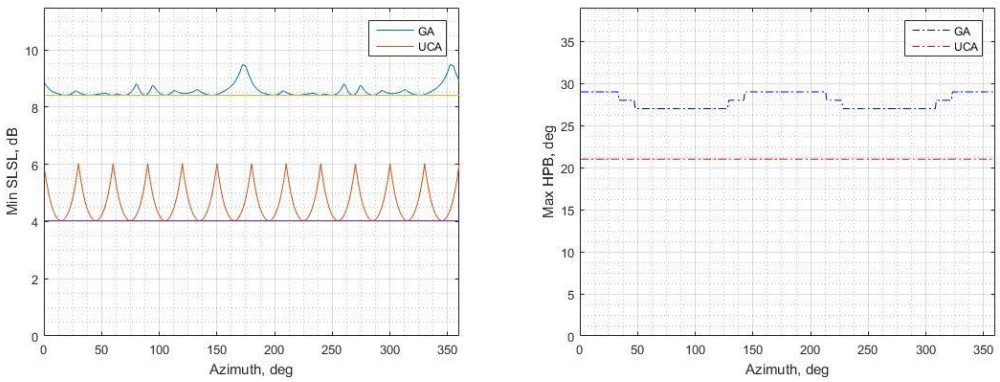

Figure 5.14: Minimum SLSL and Maximum HPB of GA Based on SLSL without HPB Constraint and UCA for 12 Sensors

Figure 5.14 shows that while the minimum SLSL of UCA is 4.02 dB, it is 8.41 dB for the sensor layout of GA based on SLSL without HPB constraint for 12 sensors. Besides, HPB of the sensor array of GA and UCA are 29° and 21°. Therefore, while the genetic algorithm suppresses the side lobe levels, the half-power beamwidth of the

sensor array increases. The reason behind increasing HPB is the decrease in the aperture of the sensor array as it is illustrated in Figure 5.13.

Figure 5.15 depicts that the location estimation performance comparison of the sensor layouts given in Figure 5.13 using the acoustic sniper localization system simulator.

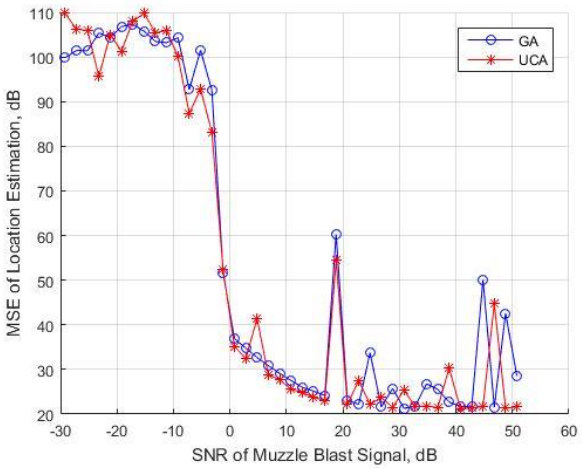

Figure 5.15: Location Estimation Performance Comparison of GA Based on SLSL without HPB Constraint and UCA for 12 Sensors in dB

In Figure 5.15, y-axis which is $MSE_{\mathrm{dB}}^{\boldsymbol{l}}$ for the shooter location estimation is calculated through the Equation 5.14. Figure 5.15 illustrates that there is no significant performance difference between two arrays for 12 sensors. Since the sensor layout of GA increases the minimum SLSL by approximately 4 dB, this improving does not affect system performance positively. Maybe, the increase in the maximum HPB might affect location estimation performance, negatively. However, this result is unexpected.

In SLSL optimizations without HPB constraint, when the number of sensors is 4 and 12, the system performance based on location estimation does not exceed the performance of UCA with the same radius. Although the side lobe suppression optimization increases the SLSL of the sensor array, HPB of sensor array increases

which affects the estimation performance, negatively. Therefore, in Section 5.4.2, the same optimizations are applied with adding HPB beamwidth constraint to investigate whether HPB affects the system performance positively or not.

5.4.2. SLSL Optimization with HPB Constraint

In SLSL optimization with HPB constraint section, the sensors of the microphone array are allowed to locate inside the circle with radius λ_{MB} and outside the circle with radius $\lambda_{\mathrm{MB}}/2$, so it is not allowed to locate inside the circle with radius $\lambda_{\mathrm{MB}}/2$ and outside the circle with radius λ_{MB}. The sensor location matrix given in Equation 2.2 is transformed into the spherical coordinate system in Equation 5.11. In Equation 5.11, $\boldsymbol{r}$ and $\boldsymbol{a}$ are the radius and angle vector of the sensor array, respectively.

The objective function for the SLSL optimization with HPB constraint is given in Equation 5.14.

$$\begin{aligned} &\max_{\boldsymbol{r},\boldsymbol{a}} \min(B_{\mathrm{SLSL}}^{\psi}) \\ &s.t. \max\ (B_{\mathrm{HPB}}^{\psi}) < 30^{\circ} \\ &\quad \frac{\lambda_{\mathrm{MB}}}{2} < r_k < \lambda_{\mathrm{MB}}, k = 1, \dots, M \\ &\quad (k-1)\frac{2\pi}{M} < a_k < k\ \frac{2\pi}{M}\ , k = 1, \dots, M \end{aligned} \tag{5.15}$$

where B_{SLSL}^{ψ} is the side lobe suppression level in ψ-incident angle, r_k and a_k are the radius and angle with respect to x-axis of the k^{th} sensor. The constraint function indicates that maximum HPB B_{HPB}^{ψ} in ψ-incident angle must be smaller than 30° since the acoustic sniper localization system gives the shooter direction to the user, by using clock position information. λ_{MB} is the wavelength of the muzzle blast signal which is approximately 68 cm, M is the number of sensors. As it is indicated in the constraint part of the optimization formula, each sensor has $\frac{2\pi}{M}$ angle interval and $\lambda_{\mathrm{MB}}/2$ radius

interval. The optimization is made for the different number of sensors (M) such as 4, 8 and 12 microphones.

5.4.2.1. Optimization of 4 Sensors

SLSL optimization with HPB constraint is made for 4 sensors using Equation 5.15, firstly. The sensor locations of GA and UCA are depicted in Figure 5.16.

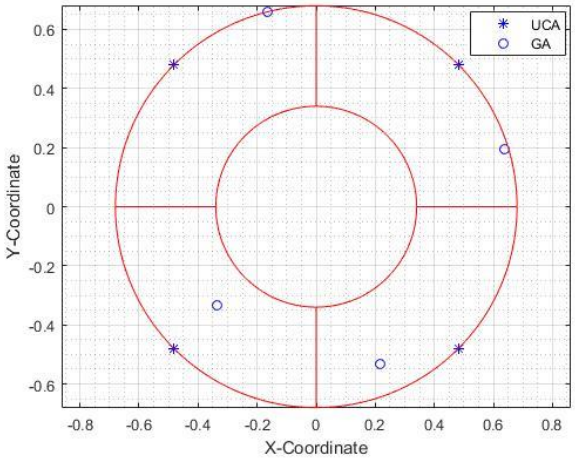

Figure 5.16: Sensor Location Demonstration of GA Based on SLSL with HPB Constraint and UCA for 4 Sensors in meters

In Figure 5.16, sensor locations of the GA and UCA are indicated with 'o' and '*' blue colored symbols, respectively. The red lines show the restricted borders of each sensor. The sensor locations demonstrated in Figure 5.16 are given in Table 5.4.

Table 5.4: The Sensor Locations of GA Based on SLSL with HPB Constraint and UCA for 4 Sensors

Array Type	Radius Vector($\boldsymbol{r}$), meters	Angle Vector($\boldsymbol{a}$), radians
UCA	$\lambda_{\mathrm{MB}}[1\ 1\ 1\ 1]^T$	$\frac{\pi}{180°}[45°\ 135°\ 225°\ 315°]^T$
GA	$\lambda_{\mathrm{MB}}[0.98\ 1\ 0.69\ 0.85]^T$	$\frac{\pi}{180°}[16°\ 104°\ 225°\ 292°]^T$

The minimum SLSL and maximum HPB for the GA and UCA concerning the incident azimuth angle are illustrated in Figure 5.17.

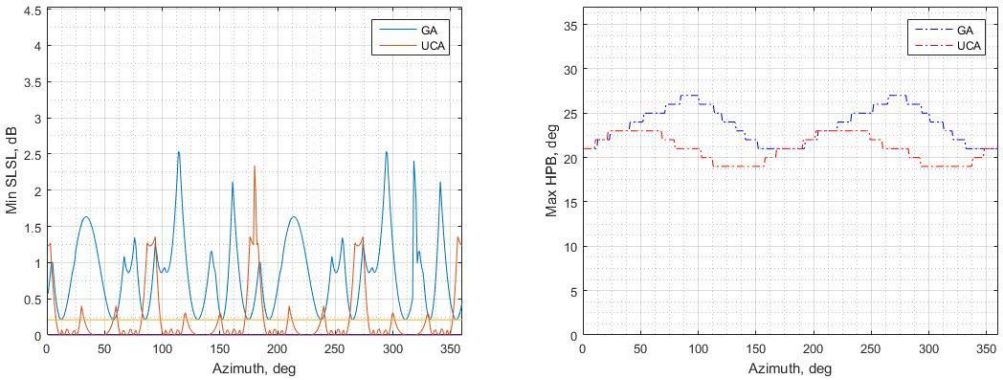

Figure 5.17: Minimum SLSL and Maximum HPB of GA Based on SLSL with HPB Constraint and UCA for 4 Sensors

Figure 5.17 shows that while there is no side lobe suppression for UCA, minimum SLSL is 0.21 dB for the sensor layout of GA based on SLSL with HPB constraint for 4 sensors. Besides, HPB of the sensor array of GA and UCA is 27° and 21°. The reason behind increasing HPB is the decrease in the aperture of the sensor array as it is illustrated in Figure 5.16. Figure 5.18 depicts that the location estimation performance comparison of the sensor layouts given in Figure 5.16 using the acoustic sniper localization system simulator.

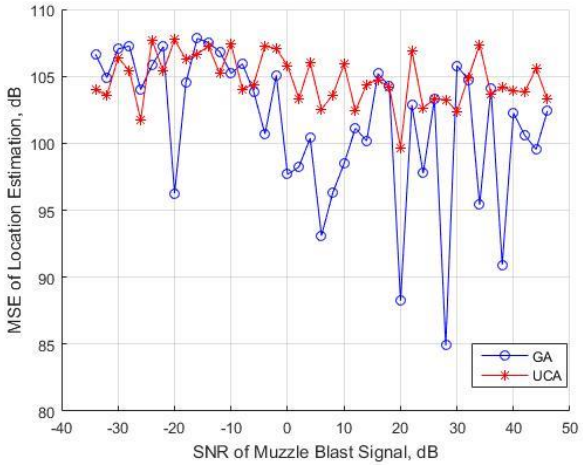

Figure 5.18: Location Estimation Performance Comparison of GA Based on SLSL without HPB Constraint and UCA for 4 Sensors in dB

In Figure 5.18, y-axis which is $MSE_{\mathrm{dB}}^{\boldsymbol{l}}$ for the shooter location estimation is calculated through the Equation 5.14. Figure 5.18 illustrates that there is no significant performance difference between two arrays since the sensor layout of GA increases the minimum SLSL by only 0.21 dB, the increase in the maximum HPB affects location estimation performance, negatively. Although the location estimation performance for the sensor layout of GA seems better, the estimation regions are not enough recognizable as threshold region and asymptotic regions while SNR increases. Therefore, they are the expected results.

5.4.2.2. Optimization of 8 Sensors

SLSL optimization with HPB constraint is made for 8 sensors using Equation 5.15, secondly. The sensor locations of GA and UCA are depicted in Figure 5.19.

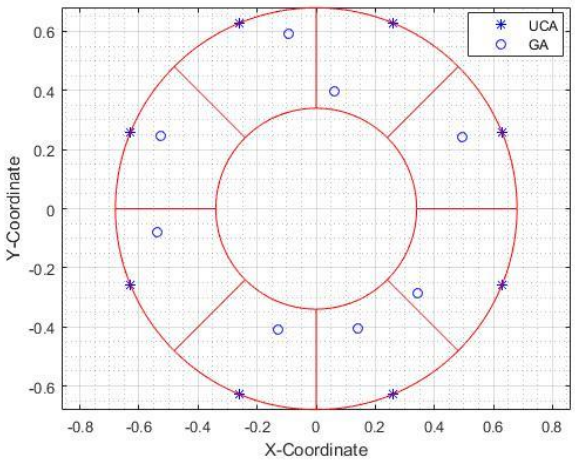

Figure 5.19: Sensor Location Demonstration of GA Based on SLSL with HPB Constraint and UCA for 8 Sensors in meters

In Figure 5.19, sensor locations of the GA and UCA are indicated with ‘o’ and ‘*’ blue colored symbols, respectively. The red lines show the restricted borders of each sensor. The sensor locations demonstrated in Figure 5.19 are given in Table 5.5.

Table 5.5: The Sensor Locations of GA Based on SLSL with HPB Constraint and UCA for 8 Sensors

Array Type	Radius Vector($\boldsymbol{r}$), meters	Angle Vector($\boldsymbol{a}$), radians
UCA	$\lambda_{\mathrm{MB}}[1\ 1 \ldots 1\ ]^T$	$\frac{\pi}{180°}[23°\ 68°\ \ldots\ 338°]^T$
GA	$\lambda_{\mathrm{MB}}[0.81\ 0.59\ 0.88\ 0.85$ $0.8\ 0.63\ 0.63\ 0.66]^T$	$\frac{\pi}{180°}[26°\ 81°\ 99°\ 155°$ $188°\ 253°\ 289°\ 320°]^T$

The minimum SLSL and maximum HPB for the GA and UCA concerning the incident azimuth angle are illustrated in Figure 5.20.

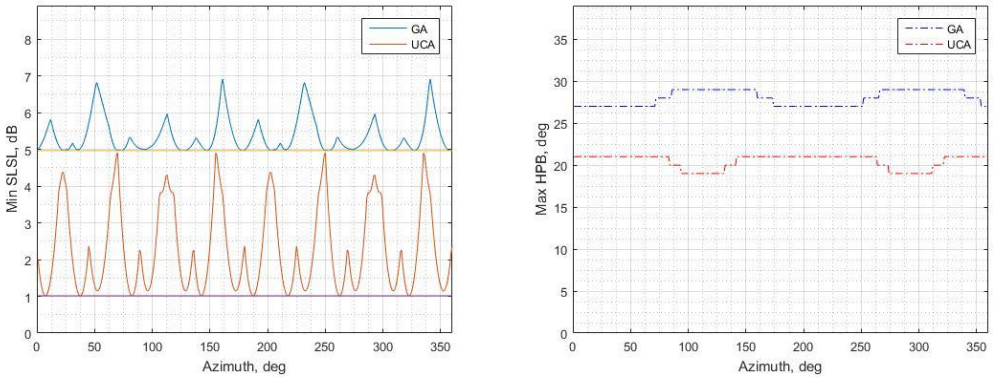

Figure 5.20: Minimum SLSL and Maximum HPB of GA Based on SLSL with HPB Constraint and UCA for 8 Sensors

Figure 5.20 shows that while the minimum SLSL of UCA is 1.11 dB, it is 4.97 dB for the sensor layout of GA based on SLSL with HPB constraint for 8 sensors. Besides, HPB of the sensor array of GA and UCA is 29° and 21°. Moreover, Figure 5.21 depicts that the location estimation performance comparison of the sensor layouts given in Figure 5.19 using the acoustic sniper localization system simulator.

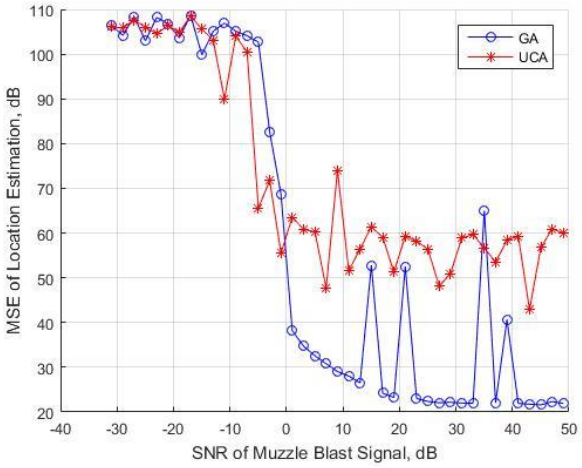

Figure 5.21: Location Estimation Performance Comparison of GA Based on SLSL with HPB Constraint and UCA for 8 Sensors in dB

In Figure 5.21, y-axis which is $MSE_{\mathrm{dB}}^{\boldsymbol{l}}$ for the shooter location estimation is calculated through the Equation 5.14. Figure 5.21 illustrates that the location estimation performance of the sensor layout of the GA exceeds the performance of UCA. At the SNR values which are lower than 0 dB, there is no significant difference between two sensor arrays. However, especially in the asymptotic region, the performance of the optimized sensor layout is much better since the minimum SLSL of the optimized sensor layout is approximately 3.8 dB more than the minimum SLSL of the UCA with the same radius. Although the HPB of the optimized sensor layout is quite larger than the HPB of UCA, side lobe suppression seems to be more dominant. Besides, HPB constraint causes the minimum SLSL to decrease by 1.3 dB. However, this decrease does not affect the location estimation performance, negatively.

5.4.2.3. Optimization of 12 Sensors

The result of this section is similar to the results of Section 5.4.1.3. Besides, to compare the reliability of the simulator, the location estimation performance comparison is done in Figure 5.22, by the same sensor arrays given in Figure 5.13.

The estimation performance is quite similar to Figure 5.15. Some small changes is the result of the gross error in the location estimation.

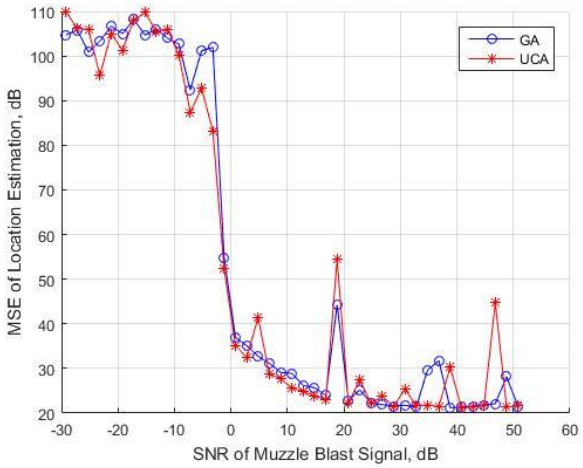

Figure 5.22: Location Estimation Performance Comparison of GA Based on SLSL with HPB Constraint and UCA for 12 Sensors

In Figure 5.22, y-axis which is $MSE_{\mathrm{dB}}^{\boldsymbol{l}}$ for the shooter location estimation is calculated through the Equation 5.14. In SLSL optimizations with HPB constraint, when the number of sensors is 4 and 12, the system performance based on location estimation does not exceed the performance of UCA with the same radius alike SLSL optimization without HPB constraint. Therefore, in Section 5.5, the optimizations based on shooter location estimation for the different number of sensors are applied to investigate the location estimation system performance.

5.5. Sensor Layout Optimization Based on Shooter Location Estimation

In most of the array optimization applications, the main aim is to design an array that increases the accuracy of the DOA estimation of the received signal. Since there are two distinctive received signals such as muzzle blast and shockwave signals that are

special to sniper localization systems, the optimization in this section will be based on the location estimation information which is the combination of all information which can be regarded as simulation-based optimization (Law et al., 2002). In optimization criteria, the sensors of the microphone array are allowed to locate inside the circle with radius λ_{SW}. The sensor location matrix given in Equation 2.2 is transformed into the spherical coordinate system in Equation 5.11. The reason for choosing the circle with radius λ_{SW} is to make optimization with the smallest aperture given in Table 1. In Equation 5.11, $\boldsymbol{r}$ and $\boldsymbol{a}$ are the radius and angle vector of the sensor array, respectively.

The objective function for the optimization of the sensor layout based on the shooter location estimation is given in Equation 5.16.

$$\begin{aligned} &\min_{\boldsymbol{r},\boldsymbol{a}} \frac{1}{K}\sum_{n=1}^{K}\left\|\hat{\boldsymbol{l}}_n - \boldsymbol{l}_n\right\|^2 \\ &\quad s.t.\, 0 < r_k < \lambda_{\mathrm{SW}}, k = 1, \dots, M \\ &\qquad (k-1)\frac{2\pi}{M} < a_k < k\,\frac{2\pi}{M}\,, k = 1, \dots, M \end{aligned} \tag{5.16}$$

where $\hat{\boldsymbol{l}}_n$ and $\boldsymbol{l}_n$ are the estimate and true DOA for the deterministic muzzle blast signal model respectively, $\|.\|$ represents the L-2 norm operator, *K* is Monte Carlo simulation number, r_k and a_k are the radius and angle with respect to x-axis of k^{th} sensor. λ_{SW} is the wavelength of the shockwave signal which is approximately 11 cm, *M* is the number of sensors, Monte Carlo simulation number is assigned as 1000 iterations which are specified in Section 6.3. As it is indicated in the constraint part of the optimization formula, each sensor has $\frac{2\pi}{M}$ angle interval. Furthermore, the optimization is made for the different number of sensors such as 4, 8 and 12 microphones.

5.5.1. Optimization of 4 Sensors

The optimization based on shooter location estimation is made for 4 microphones using Equation 5.16, firstly. The sensor locations of GA and UCA based on shooter location estimation are depicted in Figure 5.23.

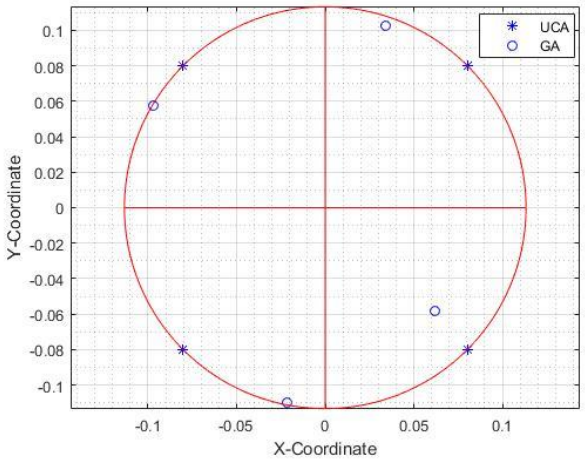

Figure 5.23: Sensor Locations of GA and UCA Based on Location Estimation for 4 Sensors in meters

In Figure 5.23, sensor locations of GA based on location estimation and UCA are indicated with 'o' and '*' blue colored symbols, respectively. The red lines show the restricted borders of each sensor. The sensor locations demonstrated in Figure 5.23 are given in Table 5.6.

Table 5.6: The Sensor Locations of GA and UCA Based on Location Estimation for 4 Sensors

Array Type	Radius Vector($\boldsymbol{r}$), meters	Angle Vector($\boldsymbol{a}$), radians
UCA	$\lambda_{\mathrm{SW}}[1\ 1\ 1\ 1]^T$	$\frac{\pi}{180^\circ}[45^\circ\ 135^\circ\ 225^\circ\ 315^\circ]^T$
GA	$\lambda_{\mathrm{SW}}[0.95\ 0.99\ 0.99\ 0.75\ ]^T$	$\frac{\pi}{180^\circ}[71^\circ\ 149^\circ\ 259^\circ\ 317^\circ]^T$

Figure 5.24 depicts that the location estimation performance comparison of the sensor layouts given in Figure 5.23 using the acoustic sniper localization system simulator given in Chapter 2. In Figure 5.24, y-axis which is $MSE_{\mathrm{dB}}^{\boldsymbol{l}}$ for the shooter location estimation is calculated through the Equation 5.14.

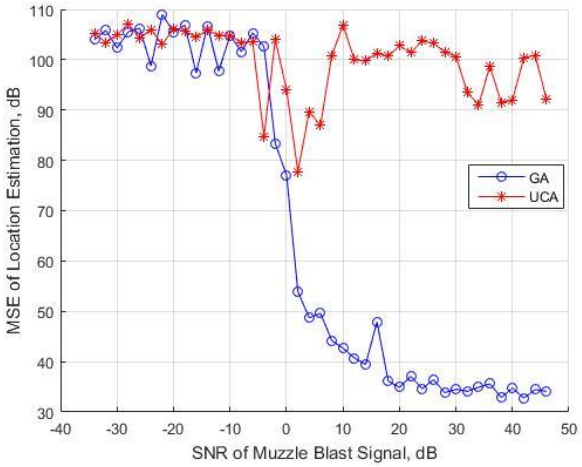

Figure 5.24: Performance Comparison of GA Based on Location Estimation and UCA for 4 Sensors in dB

Figure 5.24 illustrates that the location estimation performance of the sensor layout of the GA exceeds the performance of UCA in the threshold and asymptotic region. Especially while SNR of the muzzle blast is bigger than 0 dB, the sensor layout of GA reveals better performance. To investigate the reason behind the difference between estimation performances of two arrays, muzzle blast and shockwave estimation performance of both arrays are analyzed in Figure 5.25. As it is described in Section 5.2, while the SNR of shockwave signal is constant as 25 dB, the SNR of muzzle blast signal changes from -40 to 40 dB.

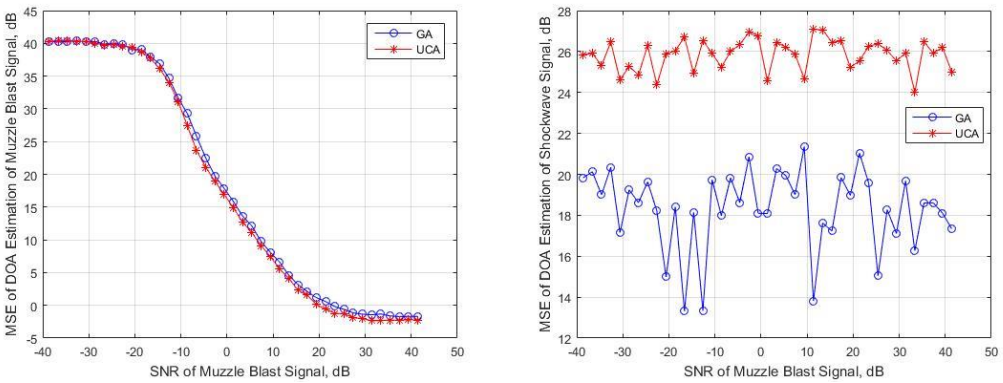

Figure 5.25: Performance Comparison of GA Based on Muzzle Blast and Shockwave Azimuth Estimations and UCA for 4 Sensors in dB

In Figure 5.25, y-axis of both figures which is $MSE_{\mathrm{dB}}^{\theta}$ for the DOA estimation of acoustic signals is calculated through the Equation 5.17.

$$MSE_{\mathrm{dB}}^{\theta} = 10\log\left(\frac{180^{\circ}}{K\pi}\sum_{n=1}^{K}\left|\hat{\theta}_n - \theta_n\right|^2\right) \tag{5.17}$$

where $\hat{\theta}_n$ and θ_n are the estimate and true DOA estimation of acoustic signals respectively, *K* is the Monte Carlo simulation number. In each Monte Carlo iteration, the location of the shooter is chosen randomly as it is indicated in Equation 2.8. The SPL of the muzzle blast signal and shockwave signals are taken as constant whose value will be calculated in Section 5.2. Therefore, true azimuth angle of the muzzle blast signal is uniformly distributed in the interval [0, 2π). The azimuth angle of the shockwave signal is arranged by the simulator using the azimuth angle of the muzzle blast signal.

Figure 5.25 illustrates that while there is no significant performance difference between two arrays for MSE of muzzle blast signal, the sensor layout of GA gives better performance in the direction estimation of shockwave signal. Therefore, the difference between the location estimation performances of two arrays is the consequence of the shockwave performance difference. Figure 5.26 gives the side lobe suppression level (SLSL) and half-power beamwidth (HPB) of the sensor arrays for all incident angles.

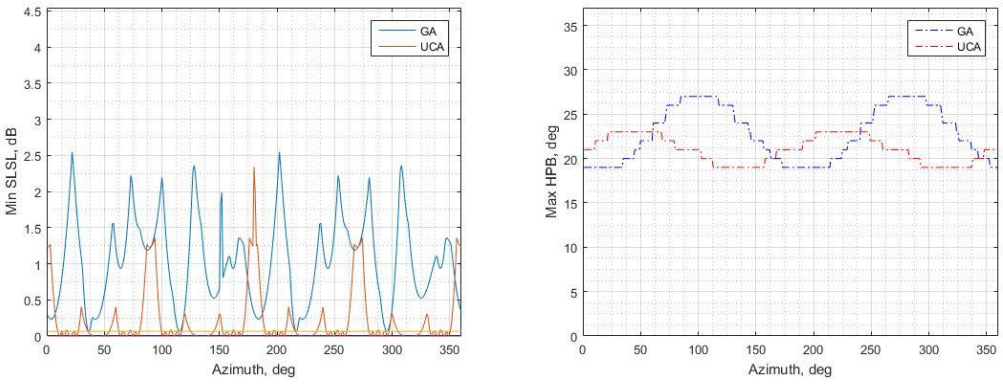

Figure 5.26: SLSL and HPB Comparison of GA Based on Location Estimation and UCA for 4 Sensors

As it is seen in Figure 5.26, although the minimum SLSL of two arrays are similar to each other, it is bigger than the SLSL of UCA by 2 dB for some incident angles. Besides, the HPB of two arrays depends on the incident wave angles and there is no significant difference between HPB performances of two arrays.

5.5.2. Optimization of 8 Sensors

The optimization based on shooter location estimation is made for 8 microphones using Equation 5.16, secondly. The sensor locations of GA and UCA based on shooter location estimation are depicted in Figure 5.27.

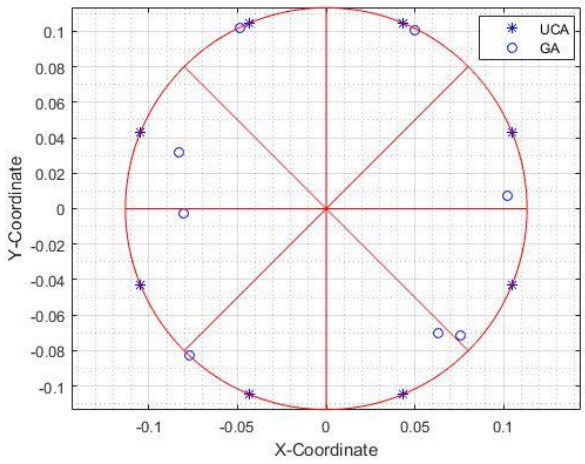

Figure 5.27: Sensor Locations of GA and UCA Based on Location Estimation for 8 Sensors in meters

In Figure 5.27, sensor locations of GA based on location estimation and UCA are indicated with ‘o’ and ‘*’ blue colored symbols, respectively. The red lines show the restricted borders of each sensor. The sensor locations demonstrated in Figure 5.27 are given in Table 5.7.

Table 5.7: The Sensor Locations of GA and UCA Based on Location Estimation for 8 Sensors

Array Type	Radius Vector($\boldsymbol{r}$), meters	Angle Vector($\boldsymbol{a}$), radians
UCA	$\lambda_{\mathrm{SW}}[1\ 1 \ldots 1\ ]^T$	$\frac{\pi}{180°}[23°\ 68°\ \ldots\ 338°]^T$
GA	$\lambda_{\mathrm{SW}}[°.9\ 0.99\ 0.99\ 0.78\ 0.71\ 0.99\ 0.83\ 0.92]^T$	$\frac{\pi}{180°}[4°\ 64°\ 115°\ 159°\ 182°\ 227°\ 312°\ 317°]^T$

Figure 5.28 depicts that the location estimation performance comparison of the sensor layouts given in Figure 5.27 using the acoustic sniper localization system simulator given in Chapter 2.

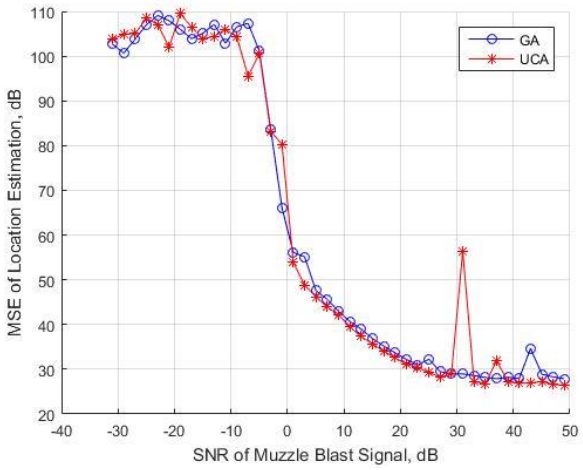

Figure 5.28: Performance Comparison of GA Based on Location Estimation and UCA for 8 Sensors in dB

In Figure 5.28, y-axis which is $MSE_{\mathrm{dB}}^{\boldsymbol{l}}$ for the shooter location estimation is calculated through the Equation 5.14. Figure 5.28 illustrates that the location estimation performance of two sensor layouts are similar to each other. To investigate the reason behind estimation performances of two arrays, muzzle blast and shockwave estimation performance of both arrays are analyzed in Figure 5.29. As it is described in Section 5.2, while the SNR of shockwave signal is constant as 25dB, the SNR of muzzle blast

signal changes from -40 to 40 dB. Therefore, x-axis of each figure given below is the SNR value of the muzzle blast signal.

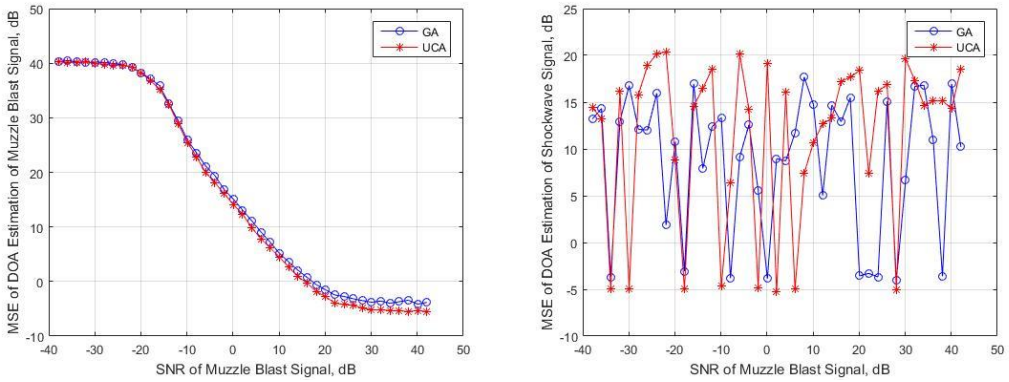

Figure 5.29: Performance Comparison of GA Based on Muzzle Blast and Shockwave Direction Estimations and UCA for 8 Sensors in dB

In Figure 5.29, y-axis of both figures which is $MSE_{\mathrm{dB}}^{\theta}$ for the DOA estimation of acoustic signals is calculated through the Equation 5.17. As it is seen in Figure 5.29, the direction estimation of muzzle blast and shockwave signals are similar to each other. Therefore, location estimation performances of two arrays given in Figure 5.28 are the expected results by considering Figure 5.29.

5.5.3. Optimization of 12 Sensors

The optimization based on shooter location estimation is made for 12 microphones using Equation 5.16, lastly. The sensor locations of GA and UCA based on shooter location estimation are depicted in Figure 5.30.

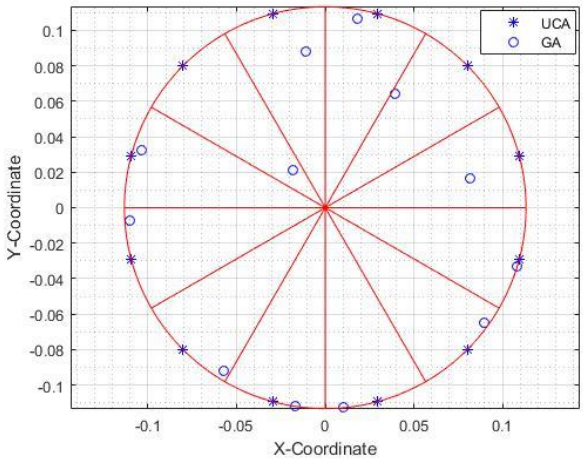

Figure 5.30: Sensor Locations of GA and UCA Based on Location Estimation for 12 Sensors in meters

In Figure 5.30, sensor locations of GA based on location estimation and UCA are indicated with 'o' and '*' blue colored symbols, respectively. The red lines show the restricted borders of each sensor. The sensor locations demonstrated in Figure 5.30 are given in Table 5.8.

Table 5.8: The Sensor Locations of GA and UCA Based on Location Estimation for 12 Sensors

Array Type	Radius Vector($\boldsymbol{r}$), meters	Angle Vector($\boldsymbol{a}$), radians
UCA	$\lambda_{\mathrm{MB}}[1\ 1 \ldots 1\ ]^T$	$\frac{\pi}{180°}[15°\ 45°\ \ldots\ 345°]^T$
GA	$\lambda_{\mathrm{MB}}[0.74\ 0.66\ 0.96\ 0.79\ 0.25\ 0.96\ 0.98\ 0.96\ \ 1\ \ 1\ \ 0.98\ \ 1]^T$	$\frac{\pi}{180°}[11°\ 58°\ 80°\ 97°\ 130°\ 163°\ 184°\ 238°\ 261°\ 275°\ 324°\ 343°]^T$

Figure 5.31 depicts that the location estimation performance comparison of the sensor layouts given in Figure 5.30 using the acoustic sniper localization system simulator given in Chapter 2.

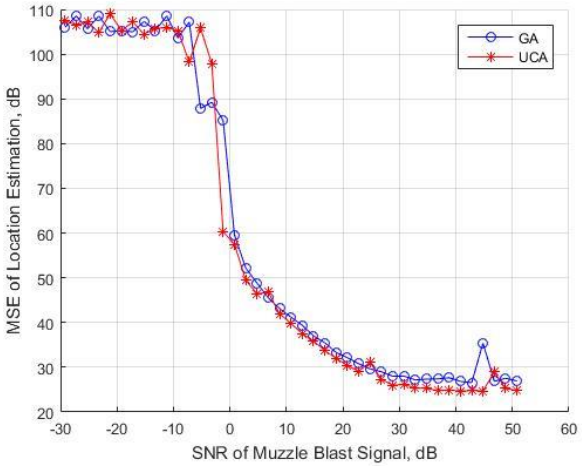

Figure 5.31: Performance Comparison of GA Based on Location Estimation and UCA for 12 Sensors

In Figure 5.31, y-axis which is $MSE_{\mathrm{dB}}^{\boldsymbol{l}}$ for the shooter location estimation is calculated through the Equation 5.14. Figure 5.31 illustrates that the location estimation performances of two sensor layouts are similar to each other. To investigate the reason behind estimation performances of two arrays, muzzle blast and shockwave estimation performance of both arrays are analyzed in Figure 5.32. While the SNR of shockwave signal is constant as 25dB, the SNR of muzzle blast signal changes from -40 to 40 dB in Figure 5.32.

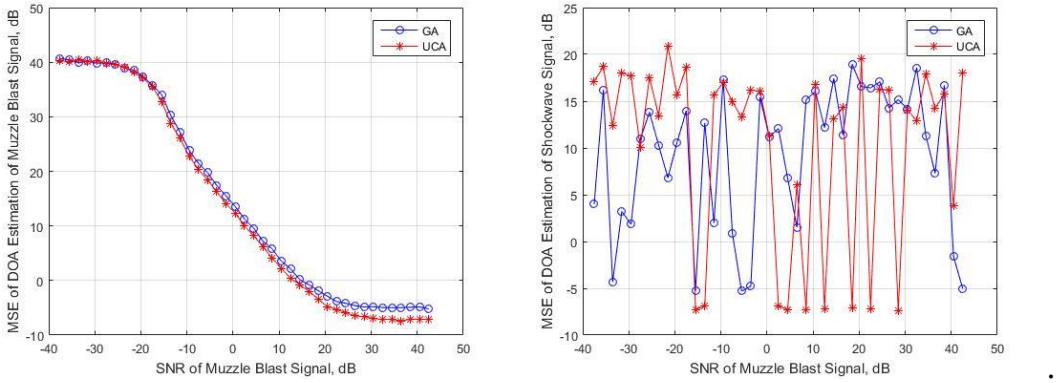

Figure 5.32: Performance Comparison of GA Based on Muzzle Blast and Shockwave Direction Estimations and UCA for 12 Sensors in dB

In Figure 5.32, y-axis of both figures which is $MSE_{\mathrm{dB}}^{\theta}$ for the DOA estimation of acoustic signals is calculated through the Equation 5.17. As it is seen in Figure 5.32, the DOA of muzzle blast and shockwave signals are similar to each other. Therefore, location estimation performances of two arrays given in Figure 5.31 are the expected results by considering Figure 5.32.

CHAPTER 6

CONCLUSION AND FUTURE WORK

6.1. Conclusion

In recent years, besides underwater acoustic applications, air acoustic detection and localization systems that are emerged from laboratory study and practiced into real-life applications have had significant importance. Estimating the direction of air targets such as a bullet, muzzle blast, drone, or anti-tank guided missile more accurately is one of the priorities in modern warfare. So, the acoustic sniper localization system is one of the most common and popular applications of modern warfare. This thesis proposes a general estimation and optimization framework for the sniper localization system.

This thesis concerns the sensor layout optimization for the sniper localization systems using the genetic algorithm. There are three different criteria to make optimization for the different number of sensors as 4, 8 and 12. These criteria are minimum side lobe suppression without half-power beamwidth constraint, minimum side lobe suppression with half-power beamwidth constraint, and minimizing location estimation error. The optimization results are verified comparing the performance of the sensor layout with the performance of UCA at the end of each optimization section. The simulation results show that there is no remarkable performance difference between minimum side lobe suppression without half-power beamwidth constraint, and minimum side lobe suppression with half-power beamwidth constraint. However, the optimization results of both sections for 8 number of sensors outperform UCA. When the number of sensors is 4 and 12, the location estimation performances of the optimized arrays are similar to the performance of UCA. Furthermore, the optimization using the genetic algorithm is made with a cost function which is mean

squared error of location estimation for the different number of sensors as 4, 8 and 12. The results of shooter location based optimization illustrate that while there is no significant difference between the location estimation performances of the optimized arrays and UCA for 8 and 12 sensors, the performance of the optimized sensor layout with 4 sensors exceeds the performance of UCA. Since the sensors of the acoustic sniper localization systems are quite expensive, the overall result is to use the optimized sensor layout with 4 sensors illustrated below.

Figure 6.1: Sensor Displacement of 4 Optimized Sensors

6.2. Future Work

There are some future works related to this thesis considering the sniper detection system concept as implementing different DOA estimation algorithms and range estimation algorithms and optimization criteria as using a different objective function as changing the angle of an incident wave from azimuthal angle to elevational angle.

For the sniper detection system concept, only DAS beamforming technique is implemented for the estimation framework. Apart from this technique, other DOA techniques can be implemented to compare algorithm performance for the given array layouts. Also, the range estimation is made using the Ferret Equation which is valid especially for a lower distance than 500m. By classifying the caliber and using the time difference of arrival between muzzle blast and shockwave and the miss distance information, range estimation can be improved.

For the optimization concept, the optimization can also be made changing the angle of the incident wave. In the optimization part of the thesis, the sensors are located on a planar region and it is assumed that the incident wave comes from the same planar with the sensor layout. This optimization criterion can be improved by changing the incident wave as being perpendicular to the planar region of the sensor layout

REFERENCES

Abel, J. S. (1990, April). Optimal sensor placement for passive source localization. In International Conference on Acoustics, Speech, and Signal Processing (pp. 2927-2930). IEEE.

Aguilar, J. R. (2013, October). Gunshot location systems the transfer of the sniper detection technology from military to civilian applications. In 2013 47th International Carnahan Conference on Security Technology (ICCST) (pp. 1-6). IEEE.

Anderson, M. J., Budwig, R. S., Line, K. S., & Frankel, J. G. (2002, October). Use of acoustic radiation pressure to concentrate small particles in an air flow. In 2002 IEEE Ultrasonics Symposium, 2002. Proceedings. (Vol. 1, pp. 481-484). IEEE.

Andradóttir, S. (1998, December). A review of simulation optimization techniques. In 1998 Winter Simulation Conference. Proceedings (Cat. No. 98CH36274) (Vol. 1, pp. 151-158). IEEE.

Arabas, J., Michalewicz, Z., & Mulawka, J. (1994, June). GAVaPS-a genetic algorithm with varying population size. In Proceedings of the First IEEE Conference on Evolutionary Computation. IEEE World Congress on Computational Intelligence (pp. 73-78). IEEE.

Aselsan (n.d.). Retrieved December 23, 2019, from https://www.aselsan.com.tr/SPOT_Atis_Yeri_Hedef_Tespit_Sistemi_3336.pdf.

Athley, F. (2005). Threshold region performance of maximum likelihood direction of arrival estimators. IEEE Transactions on Signal Processing, 53(4), 1359-1373.

Audible. (n.d.). Retrieved November 5, 2019, from http://www.smartereveryday.com/audible.

Bass, H. E., Sutherland, L. C., & Zuckerwar, A. J. (1990). Atmospheric absorption of sound: Update. The Journal of the Acoustical Society of America, 88(4), 2019-2021.

Bass, H. E., Sutherland, L. C., Zuckerwar, A. J., Blackstock, D. T., & Hester, D. M. (1995). Atmospheric absorption of sound: Further developments. The Journal of the Acoustical Society of America, 97(1), 680-683.

Beck, S. D., Nakasone, H., & Marr, K. W. (2011). Variations in recorded acoustic gunshot waveforms generated by small firearms. The Journal of the Acoustical Society of America, 129(4), 1748-1759.

Bedard, J., & Pare, S. (2003, September). Ferret: a small arms fire detection system: localization concepts. In Sensors, and Command, Control, Communications, and Intelligence (C3I) Technologies for Homeland Defense and Law Enforcement II (Vol. 5071, pp. 497-509). International Society for Optics and Photonics.

Benesty, J., Chen, J., Huang, Y., & Dmochowski, J. (2007). On microphone-array beamforming from a MIMO acoustic signal processing perspective. IEEE Transactions on Audio, Speech, and Language Processing, 15(3), 1053-1065.

Bohn, D. A. (1987, October). Environmental effects on the speed of sound. In Audio Engineering Society Convention 83. Audio Engineering Society.

Boomerang III. (n.d.). Retrieved November 5, 2019, from https://www.raytheon.com/capabilities/products/boomerang.

Boomerang Warrior-X. (n.d.). Retrieved November 5, 2019, from https://www.raytheon.com/capabilities/products/boomerang_warriorx.

Calderon, D. M. P., & Apolinario Jr, J. A. (2015). Shooter localization based on DoA estimation of gunshot signals and digital map information. IEEE Latin America Transactions, 13(2), 441-447.

Carter, G. C. (1977). Variance bounds for passively locating an acoustic source with a symmetric line array. The Journal of the Acoustical Society of America, 62(4), 922-926.

Carter, G. C. (1981) "Time delay estimation for passive sonar signal processing." IEEE Transactions on Acoustics, Speech, and Signal Processing 29.3 : 463-470.

Damarla, T., Kaplan, L. M., & Whipps, G. T. (2010). Sniper localization using acoustic asynchronous sensors. IEEE Sensors Journal, 10(9), 1469-1478.

Danicki, E. (2006). The shock wave-based acoustic sniper localization. Nonlinear analysis: theory, methods & applications, 65(5), 956-962.

Danicki, E., Kawalec, A., & Pietrasinski, J. (2004, April). On geometry of the acoustic sniper localization. In presented on the Symposium Capabilities of Acoustics in Air-Ground and Maritime Reconnessaince, Target Classification and Identification, organized by the NATO Sensors, Electronics and Technology Panel (SET-079/RSY), La Specia, Lerici, Italy.

Dmochowski, J., Benesty, J., & Affes, S. (2007). Direction of arrival estimation using the parameterized spatial correlation matrix. IEEE Transactions on Audio, Speech, and Language Processing, 15(4), 1327-1339.

Ears Swats. (n.d.). Retrieved November 5, 2019, from https://qinetiq-na.com/products/militaryprotection/ears/ears-swats/.

Fernandes, R. P., Apolinário, J. A., & Ramos, A. L. (2017, February). Bearings-only aerial shooter localization using a microphone array mounted on a drone. In 2017 IEEE 8th Latin American Symposium on Circuits & Systems (LASCAS) (pp. 1-4). IEEE.

Foote, K. G. (2014). Discriminating between the nearfield and the farfield of acoustic transducers. The Journal of the Acoustical Society of America, 136(4), 1511-1517.

Häcker, P., & Yang, B. (2010). Single snapshot DOA estimation. Advances in Radio Science, 8, 251-256.

He, Y., Liu, F., Wu, Z., Jin, W., & Du, B. (2010, November). Counter sniper: a localization system based on dual thermal imager. In Optoelectronic Imaging and Multimedia Technology (Vol. 7850, p. 78500V). International Society for Optics and Photonics.

He, Z., Zheng, F., Ma, Y., Kim, H. H., Zhou, Q., & Shung, K. K. (2015). A sidelobe suppressing near-field beamforming approach for ultrasound array imaging. The Journal of the Acoustical Society of America, 137(5), 2785-2790.

Kadan, F. E. (2018, May). Optimal circular array design for direction finding. In 2018 26th Signal Processing and Communications Applications Conference (SIU) (pp. 1-4). IEEE.

Kastek, M., Dulski, R., Madura, H., Trzaskawka, P., Bieszczad, G., & Sosnowski, T. (2011, September). Electro-optical system for gunshot detection: analysis, concept, and performance. In International Symposium on Photoelectronic Detection and Imaging 2011: Advances in Infrared Imaging and Applications (Vol. 8193, p. 81933W). International Society for Optics and Photonics.

Khalid, M. A., Babar, M. I. K., Zafar, M. H., & Zuhairi, M. F. (2013, November). Gunshot detection and localization using sensor networks. In 2013 IEEE International Conference on Smart Instrumentation, Measurement and Applications (ICSIMA) (pp. 1-6). IEEE.

Konak, A., Coit, D. W., & Smith, A. E. (2006). Multi-objective optimization using genetic algorithms: A tutorial. Reliability Engineering & System Safety, 91(9), 992-1007.

Law, A. M. ,& McComas, M. G. (2002, December). Simulation-based optimization. *In Proceedings of the Winter Simulation Conference* (Vol. 1, pp. 41-44). IEEE.

Lédeczi, Á., Nádas, A., Völgyesi, P., Balogh, G., Kusy, B., Sallai, J., ... & Simon, G. (2005). Countersniper system for urban warfare. ACM Transactions on Sensor Networks (TOSN), 1(2), 153-177.

Lindgren, D., Wilsson, O., Gustafsson, F., & Habberstad, H. (2010). Shooter localization in wireless microphone networks. Eurasip journal on advances in signal processing, 2010(1), 690732.

Mäkinen, T., & Pertilä, P. (2010). Shooter localization and bullet trajectory, caliber, and speed estimation based on detected firing sounds. Applied acoustics, 71(10), 902-913.

Mays, B. T. (2001). Shockwave and muzzle blast classification via joint time frequency and wavelet analysis. Army Research Lab Adelphi MD.

Maher, R. C. (2006, September). Modeling and signal processing of acoustic gunshot recordings. In 2006 IEEE 12th Digital Signal Processing Workshop & 4th IEEE Signal Processing Education Workshop (pp. 257-261). IEEE.

Maher, R. C. (2007, April). Acoustical characterization of gunshots. In 2007 IEEE Workshop on Signal Processing Applications for Public Security and Forensics (pp. 1-5). IEEE.

Oktel, U., & Moses, R. L. (2005). A Bayesian approach to array geometry design. IEEE Transactions on Signal Processing, 53(5), 1919-1923.

Patterson Jr, J. H., & Hamernik, R. P. (1997). Blast overpressure induced structural and functional changes in the auditory system. Toxicology, 121(1), 29-40.

Penn-Barwell, J. G., Sargeant, I. D., Penn-Barwell, J. G., Bennett, P. M., Fries, C. A., Kendrew, J. M., ... & Porter, K. (2016). Gun-shot injuries in UK military casualties–features associated with wound severity. Injury, 47(5), 1067-1071.

Pilarw (n.d.). RetrievedNovember,2019, from http://www.acoustic1.co.uk/?p=Defence&c=21.

Ramos, A. L., Holm, S., Gudvangen, S., & Otterlei, R. (2011, June). Delay-and-sum beamforming for direction of arrival estimation applied to gunshot acoustics. In Sensors, and Command, Control, Communications, and Intelligence (C3I) Technologies for Homeland Security and Homeland Defense X (Vol. 8019, p. 80190U). International Society for Optics and Photonics.

Raytheon. (n.d.). Retrieved November 5, 2019, from https://www.raytheon.com/.

Roes, M. G., Duarte, J. L., Hendrix, M. A., & Lomonova, E. A. (2012). Acoustic energy transfer: A review. IEEE Transactions on Industrial Electronics, 60(1), 242-248.

Sadler, D. J. (2009, November). Planar array design for low ambiguity. In 2009 Loughborough Antennas & Propagation Conference (pp. 713-716). IEEE.

Sallai, J., Völgyesi, P., Lédeczi, Á., Pence, K., Bapty, T., Neema, S., & Davis, J. R. (2013, April). Acoustic shockwave-based bearing estimation. In Proceedings of the 12th international conference on Information processing in sensor networks (pp. 217-228). ACM.

Snow, W. (1967). Survey of acoustic characteristics of bullet shock waves. IEEE Transactions on Audio and Electroacoustics, 15(4), 161-176.

Stoughton, R. (1997). Measurements of small-caliber ballistic shock waves in air. The Journal of the Acoustical Society of America, 102(2), 781-787.

Suh, K., & Hollerbach, J. (1987, March). Local versus global torque optimization of redundant manipulators. In Proceedings. 1987 IEEE International Conference on Robotics and Automation (Vol. 4, pp. 619-624). IEEE.

Vasconcelos, J. A., Ramirez, J. A., Takahashi, R. H. C., & Saldanha, R. R. (2001). Improvements in genetic algorithms. IEEE Transactions on magnetics, 37(5), 3414-3417.

Volgyesi, P., Balogh, G., Nadas, A., Nash, C. B., & Ledeczi, A. (2007, June). Shooter localization and weapon classification with soldier-wearable networked sensors. In Proceedings of the 5th international conference on Mobile systems, applications and services (pp. 113-126). ACM.

Warsitz, E., & Haeb-Umbach, R. (2005, March). Acoustic filter-and-sum beamforming by adaptive principal component analysis. In Proceedings.(ICASSP'05). IEEE International Conference on Acoustics, Speech, and Signal Processing, 2005. (Vol. 4, pp. iv-797). IEEE.

Zhang, X., Song, E., Huang, J., Liu, H., Wang, Y., Li, B., & Yuan, X. (2014). Acoustic source localization via subspace based method using small aperture MEMS arrays. Journal of Sensors, 2014.